only as strongly positive if the three reviewers independently defined them as such.

Statistical analysis. Statistical analyses were performed using the StatView statistical program (SaS, Cary, NC). We used contingency tables to analyze the relationship between FGFR1OP expression and clinicopathological variables in NSCLC patients. Tumor-specific survival curves were calculated from the date of surgery to the time of death related to NSCLC, or to the last follow-up observation. Kaplan-Meier curves were calculated for each relevant variable and for FGFR1OP expression; differences in survival times among patient subgroups were analyzed using the log-rank test. Univariate and multivariate analyses were carried out with the Cox proportional-hazard regression model to determine associations between clinicopathological variables and cancer-related mortality. First, we analyzed associations between death and possible prognostic factors including age, gender, histological type, pT-classification, pN-classification, and smoking history, taking into consideration one factor at a time. Second, multivariate Cox analysis was applied on backward (stepwise) procedures that always forced strong FGFR1OP expression into the model, along with any and all variables that satisfied an entry level of a P-value of less than 0.05. As the model continued to add factors, independent factors did not exceed an exit level of $P < 0.05$.

RNA interference assay. Using the vector-based RNA interference (RNAi) system, psiH1BX3.0, which we had established earlier to direct the synthesis of siRNAs in mammalian cells,[14] we transfected 10 μg of siRNA-expression vector with 30 μL of Lipofectamine 2000 (Invitrogen) into two lung-cancer cell lines, LC319 and SBC-5, that endogenously overexpressed FGFR1OP. The transfected cells were cultured for 5 days in the presence of appropriate concentrations of geneticin (G418). Cell numbers and viability were measured by Giemsa staining and 3-(4,5-dimethylthiazol-2-yl)-2,5-diphenyltetrazolium bromide (MTT) assay in triplicate. The target sequences of the synthetic oligonucleotides for RNAi were as follows: control-1 (EGFP, enhanced green fluorescent protein [GFP] gene, a mutant of *Aequorea victoria* GFP), 5′-GAAGCAGCACGACTTCTTC-3′; control-2 (LUC, luciferase gene from *Photinus pyralis*), 5′-CGTACGCGGAATACTTCGA-3′; control-3 (SCR, scramble chloroplast *Euglena gracilis* gene coding for the 5S and 16S rRNA), 5′-GCGCGCTTTGTAGGATTCG-3′; siRNA-FGFR1OP-1 (si-1), 5′-CCTGAAACTAGCACACTGC-3′; siRNA-FGFR1OP-2 (si-2), '5-GGTAAGAAGAAGACAAGCG-3′. To validate our RNAi system, downregulation of *FGFR1OP* expression by functional siRNA, but not by controls, was confirmed in the cell lines used for this assay.

Cell migration assay. Using FuGENE 6 Transfection Reagent (Roche Diagnostics) according to the manufacturer's instructions, we transfected COS-7 cells with plasmids expressing FGFR1OP (pCDNA3.1/myc-His-FGFR1OP) or mock plasmids (pCDNA3.1/myc-His). Transfected cells were harvested and suspended in Dulbecco's modified Eagle's medium (DMEM) without FCS. DMEM containing 10% FCS was added to each lower chamber of 24-well migration chambers (Becton Dickinson Labware) and cell suspension was added to each insert of the upper chamber. The plates of inserts were incubated for 24 h at 37°C, then subsequently extracted and stained migrated-cells on the bottom side of the membrane.

Matrigel invasion assay. COS-7 cells transfected either with plasmids expressing FGFR1OP (pCDNA3.1/myc-His-FGFR1OP) or with mock plasmids were grown to near confluence in DMEM containing 10% FCS. The cells were harvested by trypsinization, washed in DMEM without addition of serum or proteinase inhibitor, and suspended in DMEM at concentration of 1×10^5 cells/mL. Before preparing the cell suspension, the dried layer of Matrigel matrix (Becton Dickinson Labware) was rehydrated with DMEM for 2 h at room temperature. DMEM (0.75 mL) containing 10% FCS was added to each lower chamber in 24-well Matrigel invasion chambers, and 0.5 mL (5×10^4 cells) of the cell suspension was added to each insert of the upper chamber. The plates of inserts were incubated for 22 h at 37°C and the chambers were processed; cells invading through the Matrigel were fixed and stained by Giemsa as directed by the supplier (Becton Dickinson Labware).

Identification of FGFR1OP-associated proteins. Cell extracts from lung-cancer cell line LC319 were precleared by incubation at 4°C for 1 h with 100 μL of protein G-agarose beads in a final volume of 2 mL of immunoprecipitation buffer (0.5% NP-40, 50 mM Tris-HCl, 150 mM NaCl) in the presence of proteinase inhibitor. After centrifugation at 80g for 5 min at 4°C, the supernatant was incubated at 4°C with anti-FGFR1OP polyclonal antibody or normal rabbit IgG for 2 h. The beads were then collected by centrifugation at 2000g for 2 min and washed six times with 1 mL of each immunoprecipitation buffer. The washed beads were resuspended in 50 μL of Laemmli sample buffer and boiled for 5 min, and the proteins were separated in 5–20% SDS polyacrylamide gel electrophoresis (PAGE) gels (BIO RAD). After electrophoresis, the gels were stained with silver. Protein bands specifically found in extracts immunoprecipitated with anti-FGFR1OP polyclonal antibody were excised and served for matrix-assisted laser desorption/ionization-time of flight mass spectrometry (MALDI-TOF-MS) analysis (AXIMA-CFR plus, SHIMADZU BIOTECH).

ABL1 kinase assay. Recombinant FGFR1OP (Abnova Corporation) and WRNIP1 were immunoprecipitated with anti-c-myc antibodies using cell extracts from COS-7 cells transfected with plasmids expressing myc-tagged proteins (pCDNA3.1/myc-His-FGFR1OP or pCDNA3.1/myc-His-WRNIP1). Full-length human recombinant His-tagged ABL1 (Invitrogen) was incubated with the recombinant FGFR1OP or WRNIP1 in kinase assay buffer (50 mM Tris, pH 7.4, 10 mM $MgCl_2$, 2 mM dithiothreitol, 1 mM NaF, 0.2 mM ATP) for 60 min at 30°C. The reactions were terminated by the addition of Laemmli sample buffer and heating at 95°C for 5 min. We detected *in vitro* phosphorylated samples by standard SDS-PAGE and subsequent western-blotting using anti-pan-phosphotyrosine antibodies or [γ-^{32}P]-ATP incorporation assays, as reported previously.[26]

BrdU-incorporation assay. Lung-cancer A549 cells transfected with plasmids designed to express ABL1 (pCDNA3.1/myc-His-ABL1), FGFR1OP (pCDNA3.1/myc-His-FGFR1OP), or WRNIP1 (pCDNA3.1/myc-His-WRNIP1), or mock plasmids (pCDNA3.1/myc-His), were cultured for 48 h. BrdU (5-bromodeoxyuridine) solution was then added in culture medium, and the cells were incubated for 8 h and fixed; incorporated BrdU was measured using a commercially available kit (Cell Proliferation ELISA, BrdU; Roche Diagnostics, Basel, Switzerland).

Results

FGFR1OP expression in lung tumors and normal tissues. To identify target molecules for the development of novel therapeutic agents and/or biomarkers for lung cancer, we first screened a cDNA microarray consisting 27 648 genes, and found the *FGFR1OP* transcript to be overexpressed in the majority of lung cancer samples examined. We then confirmed its transactivation by semiquantitative RT-PCR experiments in nine of 14 additional NSCLC tissues and in 17 of 19 lung-cancer cell lines (Fig. 1a). Because FGFR1OP was originally identified as a fusion partner for FGFR1 in t(6;8)(q27;p11) chromosomal translocations responsible for myeloproliferative disorders (MSD), we screened *FGFR1-FGFR1OP* fusion transcripts in various lung-cancer cell lines using *FGFR1OP* and *FGFR1* specific primers.[28–30] Both *FGFR1OP* and *FGFR1* transcripts were detected in all lung-cancer cell lines examined, but neither *FGFR1OP-FGFR1* nor *FGFR1-FGFR1OP* reciprocal transcripts was detected (data not shown).

doi: 10.1111/j.1349-7006.2007.00610.x

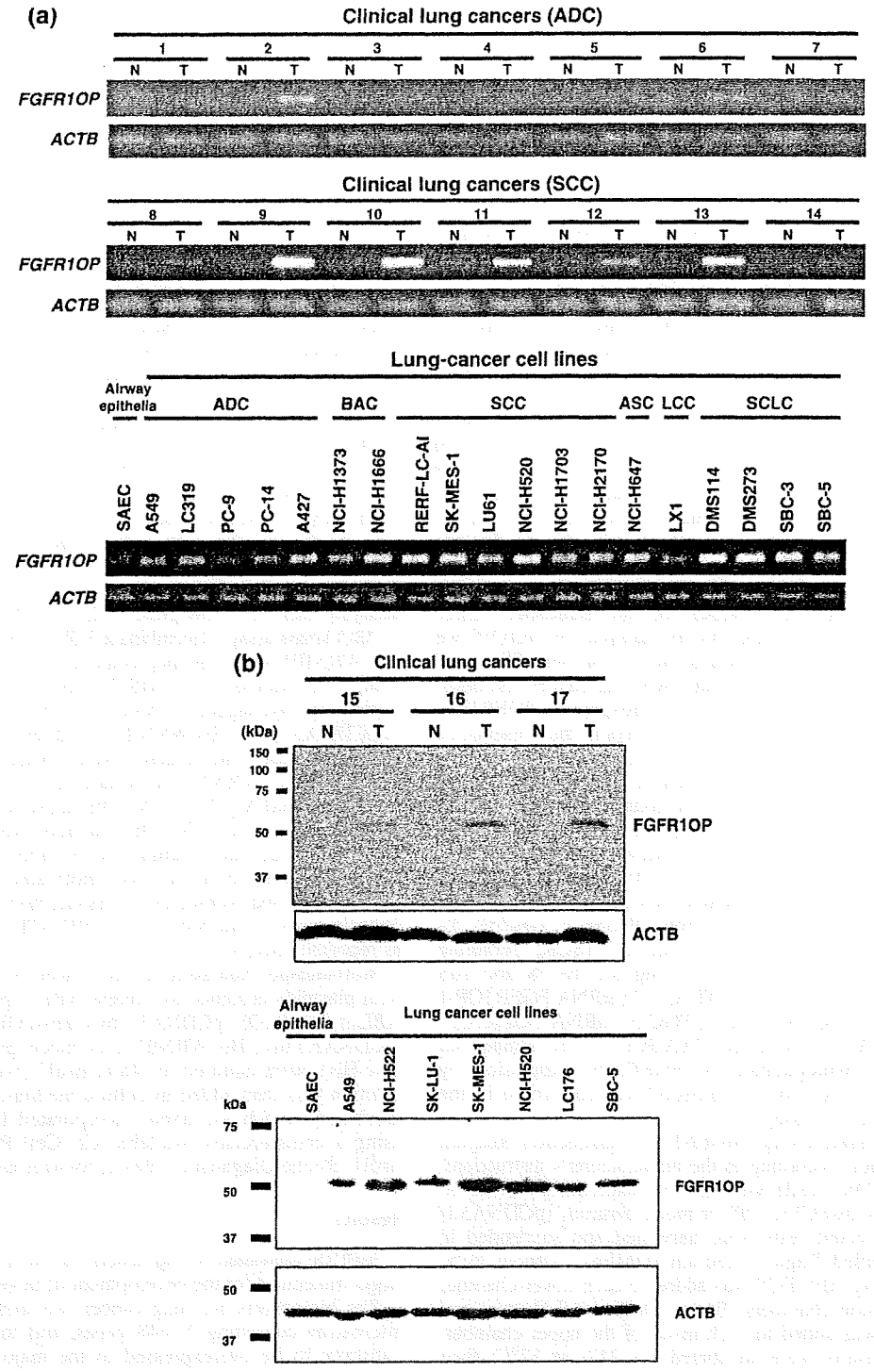

Fig. 1. Fibroblast growth factor receptor 1 oncogene partner (FGFR1OP) expression in lung cancers and normal tissues. (a) Expression of *FGFR1OP* in clinical samples of non-small cell lung cancer (NSCLC) (T) and corresponding normal lung tissues (N), examined by semiquantitative reverse transcription-polymerase chain reaction (RT-PCR) (upper panels). Expression of *FGFR1OP* in lung-cancer cell lines, detected by semiquantitative RT-PCR (lower panels). (b) Western-blot analysis of FGFR1OP protein in three representative pairs of lung-cancer tissue samples (upper panels). Western-blot analysis of FGFR1OP protein in lung-cancer cell lines (lower panels). (c) Cell-cycle dependent localization of endogenous FGFR1OP. LC319 cells were synchronized at the G1/S boundary by aphidicolin. At different time-points after the release from cell-cycle arrest, fluorescence-activated cell sorting (FACS) analysis, immunocytochemical staining was carried out. Cells were immunostained with FGFR1OP-Alexa488 (green) using anti-FGFR1OP antibody or cell nuclei (blue; 4′6′-diamidino-2-phenylindole dihydrochloride [DAPI]) at individual time points. (d) Upper panel, Northern-blot analysis of the FGFR1OP transcript in 23 normal adult human tissues. Lower panels, immunohistochemical evaluation of FGFR1OP protein in representative normal tissues and lung cancers; adult heart, liver, lung, kidney, testis and lung adenocarcinoma tissue. Magnification, ×200.

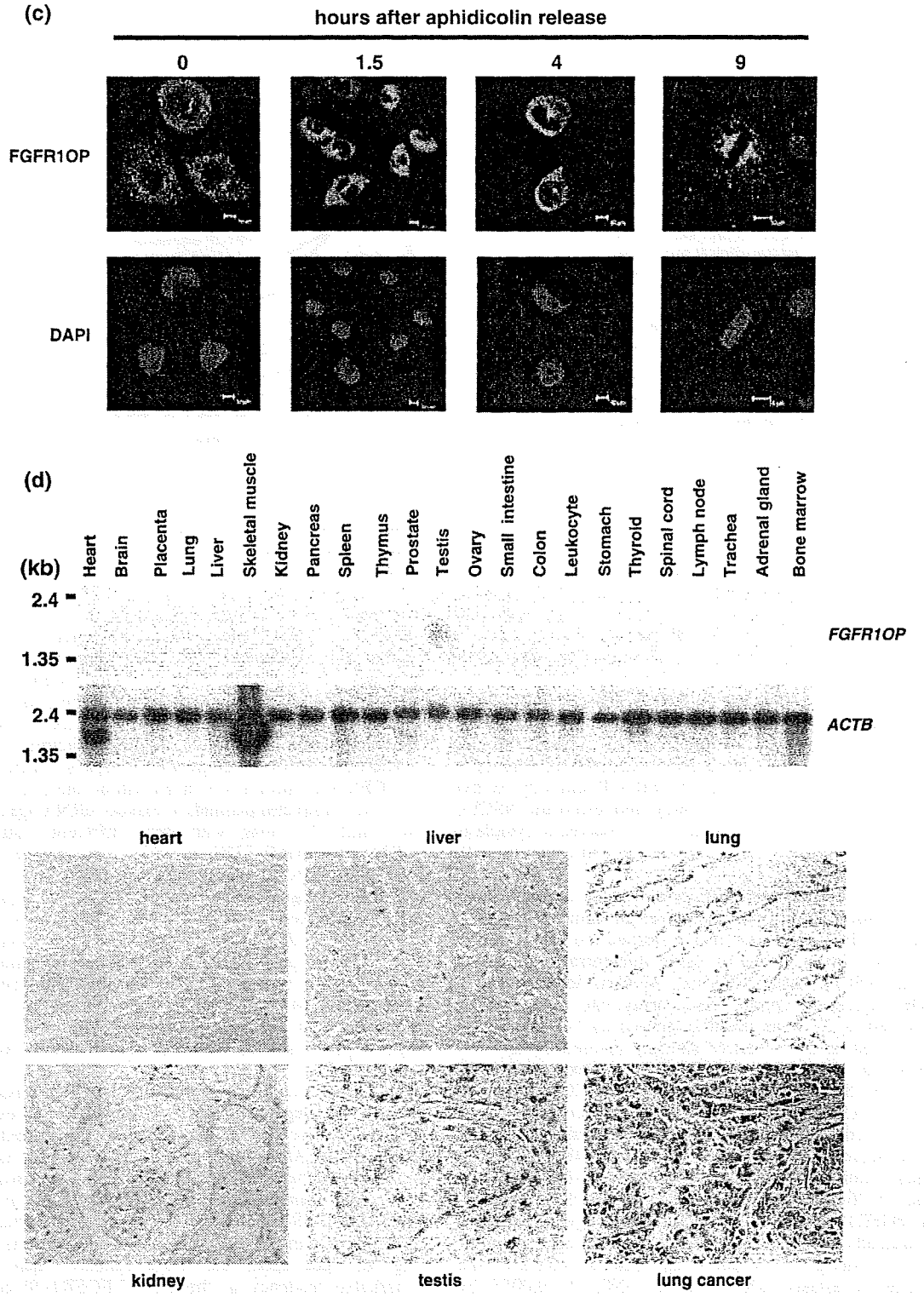

Fig. 1. *Continued*

We subsequently examined by western-blot analysis an expression of FGFR1OP protein in lung cancer tissues and cell lines, and found the increased FGFR1OP protein expression in representative pairs of clinical lung cancer tissue samples and in lung-cancer cell lines (Fig. 1b). We then carried out immunofluorescence analysis to examine the subcellular localization of endogenous FGFR1OP in lung-cancer cells. LC319 cells, synchronized using aphidicolin, were harvested for flow cytometric and immunofluorescence analyses at various time-points after release from the cell-cycle arrest. Before removal of aphidicolin

doi: 10.1111/j.1349-7006.2007.00610.x

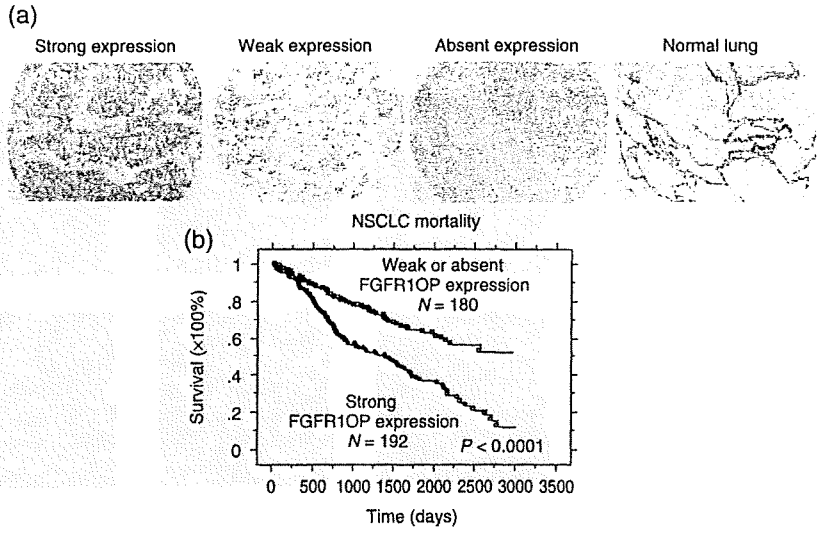

Fig. 2. Fibroblast growth factor receptor 1 oncogene partner (FGFR1OP) protein expression and its association with poorer clinical outcomes for non-small cell lung cancer (NSCLC) patients. (a) Immunohistochemical evaluation of FGFR1OP protein expression on tissue microarrays. Examples are shown for strong, weak, or absent FGFR1OP expression in lung squamous cell carcinomas, and for no expression in normal lung. Magnification, ×100. (b) Kaplan-Meier analysis of tumor-specific survival in 372 patients with NSCLCs according to the level of FGFR1OP expression ($P < 0.0001$; log-rank test).

(0 h), FGFR1OP was observed in nucleus and cytoplasm with granular appearance. At 1.5 h after release when most cells were in the S phase, FGFR1OP was stained in nucleus and cytoplasm as well as centrosome. Interestingly, FGFR1OP was detected mainly in perinucleus as well as in nucleus at 4 h when the cells started to enter the G2/M phase. At 9 h, when most cells were in the G2/M phase, FGFR1OP was localized mainly in centrosome and cytoplasm (Fig. 1c). FGFR1OP protein levels were not changed during cell cycle progression, as detected by western-blot analysis (data not shown).

Northern blot analysis using an *FGFR1OP* cDNA fragment as a probe identified a transcript of about 1.8 kb that was expressed only in the testis among 23 normal human tissues examined (Fig. 1d, upper panels). We subsequently examined the expression of FGFR1OP protein with the anti-FGFR1OP antibody on five normal tissues (heart, liver, lung, kidney, and testis) and NSCLC tissues, and found that positive staining was observed in cytoplasm and/or nucleus of primary lung cancer cells and testicular cells (Fig. 1d, lower panels).

Association of FGFR1OP overexpression with poor clinical outcome for NSCLC patients. To verify the biological and clinicopathological significance of FGFR1OP, we also examined the expression of FGFR1OP protein by means of tissue microarrays containing 372 primary NSCLC tissues (Fig. 2a). We classified a pattern of FGFR1OP expression on the tissue array into three classes, absent (scored as 0), weak positive (scored as 1+), and strong positive (scored as 2+). Positive staining (scored 2+ and 1+) was observed in 206 (86.9%) of 237 ADC cases examined, in 92 (97.9%) of 94 SCCs, in 24 (85.7%) of 28 LCCs and in 12 (92.3%) of 13 ASCs, while no staining was observed in any of the normal portions of the same tissues. Strong FGFR1OP expression (scored 2+) was observed in 116 (48.9%) of 237 ADC cases examined, 54 (57.4%) of 94 SCCs, 12 (42.9%) of 28 LCCs and 10 (76.9%) of 13 ASCs. We evaluated the association between FGFR1OP status and clinicopathological variables among surgically resected lung cancers, and found that tumor size (pT2-4 *versus* pT1; $P = 0.0031$ by Fisher's exact test) and lymph node metastasis (pN1-2 *versus* pN0; $P = 0.0056$ by Fisher's exact test) were significantly associated with the strong FGFR1OP expression (Table 1). The median survival time of patients with strong FGFR1OP-staining tumors (scored 2+) was significantly shorter than that of patients with absent and/or weak FGFR1OP-staining (scored 0 and 1+) ($P < 0.0001$ by log-rank test; Fig. 2b). We also used univariate analysis to evaluate associations between patient prognosis and other factors including age (≥65 *vs* <65), gender (male *vs* female), histological classification (other histological types *vs* adenocarcinoma), pT classification (pT2-4 *vs* pT1) and pN classification (pN1–2 *vs* pN0), smoking history (current and former smoker *vs* never-smoker), and FGFR1OP status (scored 2+ *vs* scored 0, 1+) (Table 2). Among those parameters, strong FGFR1OP expression ($P < 0.0001$), elderly ($P = 0.0375$), male gender ($P = 0.0008$), non-adenocarcinoma histological type ($P = 0.009$), advanced pT stage ($P < 0.0001$), and advanced pN stage ($P < 0.0001$) were significantly associated with poor prognosis. In multivariate analyses of prognostic factors, strong FGFR1OP expression ($P < 0.0001$) as well as elderly ($P = 0.0036$), advanced pT stage ($P = 0.0009$), and advanced pN stage ($P < 0.0001$) were significant and independent unfavorable prognostic factors (Table 2).

Effect of FGFR1OP on cell growth. To assess whether upregulation of FGFR1OP plays a role in growth or survival of lung-cancer cells, we constructed plasmids to express siRNA against *FGFR1OP* (si-1 and -2), along with three different control plasmids (siRNAs for EGFP, LUC, and SCR), and transfected them into LC319 and SBC-5 cells to suppress expression of endogenous *FGFR1OP* (Fig. 3a). The level of *FGFR1OP* expression in the cells transfected with si-1 was significantly reduced, in comparison with those with any of the three control siRNAs (Fig. 3a, upper panels). si-2 showed almost no suppressive effect on *FGFR1OP* expression. Cell viability and colony numbers measured by MTT and colony-formation assays were reduced significantly in the cells transfected with si-1 in comparison with those transfected with the other plasmid clones (Fig. 3a, lower panels).

To further examine a potential role of FGFR1OP in tumorigenesis, we prepared plasmids designed to express FGFR1OP (pcDNA3.1/myc-His-FGFR1OP) and transfected them into COS-7 cells. After confirmation of FGFR1OP expression by western-blot analysis (Fig. 3b, left panels), we carried out MTT and colony-formation assays, and found that growth of the FGFR1OP-COS-7 cells was promoted at a significant degree in comparison to the COS-7 cells transfected with the mock vector (Fig. 3b, right upper and lower panels). There was also a remarkable tendency in the COS-7-FGFR1OP cells to form larger colonies than the control cells (Fig. 3b, right lower panels), implying that FGFR1OP has an oncogenic activity in mammalian cells.

Activation of cellular migration and invasion by FGFR1OP. As the immunohistochemical analysis on tissue microarray indicated that lung cancer patients with FGFR1OP strong-positive tumors showed a shorter cancer-specific survival period than those with FGFR1OP-weak-positive and/or negative tumors, we examined a

Table 1. Association between FGFR1OP-positivity in NSCLC tissues and patients' characteristics (n = 372)

	Total (n = 372)	FGFR1OP strong expression (n = 192)	FGFR1OP weak expression (n = 142)	FGFR1OP absent expression (n = 38)	P-value strong positive *vs* weak/absent
Sex					
Male	258	141	93	24	NS
Female	114	51	49	14	
Age (years)					
<65	186	103	63	20	NS
≥65	186	89	79	18	
Histological type					
ADC	237	116	90	31	NS‡
SCC	94	54	38	2	
Others†	41	22	14	5	
pT factor					
T1	125	51	53	21	0.0031*
T2–4	247	141	89	17	
pN factor					
N0	229	105	95	29	0.0056*
N1 + N2	143	87	47	9	
Smoking history					
Never smoker	113	57	43	13	NS
Smoker	259	135	99	25	

*P < 0.05 (Fisher's exact test). †Large cell carcinoma (LCC) plus adenosquamous cell carcinoma (ASC). ‡ADC versus non-ADC (SCC and others). ADC, adenocarcinoma; NS, no significance; SCC, squamous cell carcinoma.

Table 2. Cox's proportional hazards model analysis of prognostic factors in NSCLC patients

Variables	Hazards ratio	95% CI	Unfavorable/favorable	P-value
Univariate analysis				
FGFR1OP	2.236	1.656–3.020	Strong (+)/weak (+) or (–)	<0.0001*
Age (years)	1.358	1.018–1.812	≥65/<65	0.0375*
Sex	1.776	1.270–2.484	Male/female	0.0008*
Histological type	1.470	1.101–1.962	non-ADC/ADC1	0.0090*
pT factor	2.639	1.848–3.784	T2–T4/T1	<0.0001*
pN factor	2.569	1.927–3.423	N1 + N2/N0	<0.0001*
Smoking history	1.276	0.927–1.756	smoker/non-smoker	NS
Multivariate analysis				
FGFR1OP	1.892	1.396–2.564	Strong (+)/weak (+) or (–)	<0.0001*
Age (years)	1.552	1.155–2.086	≥65/<65	0.0036*
Sex	1.382	0.955–2.000	Male/female	NS
Histological type	1.091	0.796–1.493	non-ADC/ADC	NS
pT factor	1.885	1.295–2.744	T2–4/T1	0.0009*
pN factor	2.380	1.769–3.201	N1 + N2/N0	<0.0001*

*P < 0.05. ADC, adenocarcinoma; NS, no significance.

possible role of FGFR1OP in cellular migration and invasion using cell migration and Matrigel invasion assays. Transfection of FGFR1OP-expressing plasmids (pcDNA3.1/myc-His-FGFR1OP) into COS-7 cells significantly enhanced its migration as well as invasive activity through Matrigel, compared to cells transfected with mock vector (Fig. 3c,d).

Identification of molecules interacting with FGFR1OP. To elucidate the biological mechanism of FGFR1OP in lung carcinogenesis, we attempted to identify proteins that would interact with FGFR1OP in lung cancer cells. Cell extracts from LC319 cells were immunoprecipitated with anti-FGFR1OP antibody or rabbit IgG (negative control). Following separation by SDS-PAGE, protein complexes were silver-stained. Protein bands, which were seen in immunoprecipitates by anti-FGFR1OP antibody, but not in those by rabbit IgG, were excised, trypsin-digested, and subjected to mass spectrometry analysis. Peptides from two independent protein bands matched to amino-acid sequences of WRNIP1 and ABL1. We subsequently confirmed the cognate interaction of endogenous FGFR1OP with endogenous WRNIP1 or ABL1 in LC319 cells by immunoprecipitation experiments (Fig. 4a).

***In vitro* and *in vivo* phosphorylation of WRNIP1 by ABL1.** Since ABL1 is a latent tyrosine kinase that could regulate many cellular processes including inhibition of the cell cycle progression,[40,41] we examined whether FGFR1OP or WRNIP1 could be a potential substrate for ABL1. We carried out an *in vitro* kinase assay by incubating recombinant His-tagged ABL1 protein with c-myc tagged FGFR1OP or c-myc-tagged WRNIP1 (Fig. 4b,c). Subsequent western-blot analysis using anti-pan-phosphotyrosine specific antibodies detected that WRNIP1 was phosphorylated by ABL1 tyrosine kinase (Fig. 4b, right panels), whereas there was no detectable ABL1-dependent phosphorylation of FGFR1OP (Fig. 4b, left panels). We confirmed the phosphorylation of WRNIP1 using the same assay in the presence of

doi: 10.1111/j.1349-7006.2007.00610.x

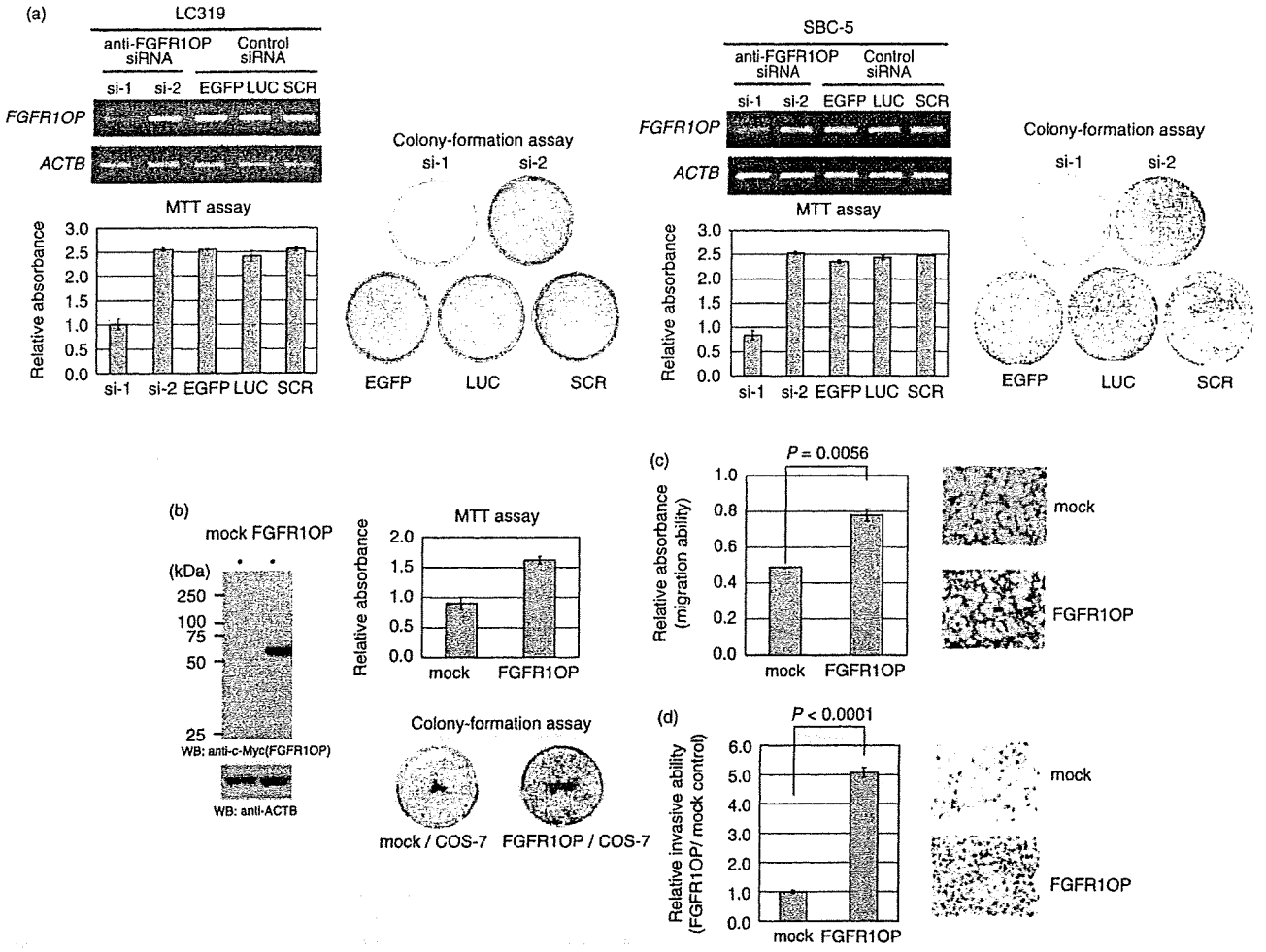

Fig. 3. Effect of fibroblast growth factor receptor 1 oncogene partner (FGFR1OP) on growth and invasive activity of cells. (a) Expression of *FGFR1OP* in response to si-FGFR1OPs (si-1 and -2) or control siRNAs (EGFP, enhanced green fluorescent protein [GFP], luciferase [LUC], or scramble [SCR]) in LC319 (left) and SBC-5 (right) cells, analyzed by semiquantitative reverse transcription-polymerase chain reaction (RT-PCR) (upper panels). Viability of LC319 or SBC-5 cells evaluated by MTT assay in response to si-1, si-2, si-EGFP, si-LUC, or si-SCR (lower panels). Colony-formation assays of LC319 and SBC-5 cells transfected with specific siRNAs or control plasmids (lower panels). All experiments were carried out in triplicate. (b) Effect of FGFR1OP on growth of COS-7 cells. Expression of FGFR1OP in COS-7 cells examined by western-blot analysis (left panels). The cells transfected with pcDNA3.1-myc-His-FGFR1OP or mock vector were each cultured in triplicate, the cell viability was evaluated by the MTT assay (right upper panel). Sizes and numbers of colonies derived from cells transfected with FGFR1OP-expressing plasmids are greater than those with mock vector (right lower panels). (c) Cell migration assay demonstrating the increased motility of COS-7 cells transfected with expression plasmids for FGFR1OP. Colorimetric measurements and Giemsa staining were shown (×200) (left and right panels). Assays were carried out three times, and each in triplicate wells. (d) Assays demonstrating the invasive nature of COS-7 cells in Matrigel matrix after transfection with expression plasmids for FGFR1OP. Giemsa staining (×200) and the number of cells migrating through the Matrigel-coated filters (left and right panels). Assays were carried out three times, and each in triplicate wells.

[γ-^{32}P]-ATP (Fig. 4c). To further examine whether WRNIP1 could be phosphorylated by ABL1 *in vivo*, we exogenously overexpressed both c-myc-tagged WRNIP1 and Flag-tagged ABL1 in COS-7 cells, and subsequently immunoprecipitated the WRNIP1 with anti-c-myc antibody and immunoblotted it using anti-pan-phosphotyrosine antibody. Expectedly, tyrosine phosphorylation of WRNIP1 by ABL1 was detected (Fig. 4d). These data suggested that WRNIP1 was likely to be a cognate substrate of ABL1 kinase.

Inhibition of ABL1-dependent phosphorylation of WRNIP1 by FGFR1OP. To elucidate the function of the interaction between FGFR1OP and WRNIP1/ABL1 in lung carcinogenesis, we examined the subcellular localization of these proteins in lung cancer cells, A549. Immunocytochemical analysis using anti-FGFR1OP and anti-WRNIP1/ABL1 antibodies demonstrated that endogenous FGFR1OP was colocalized with endogenous WRNIP1 and ABL1 mainly in perinucleus as well as in nucleus at S ~ G2/M phase (Fig. 5a).

To determine whether FGFR1OP could affect phosphorylation of WRNIP1 by ABL1, we carried out *in vitro* kinase assay by incubating c-myc tagged WRNIP1 with His-tagged ABL1 in the absence or presence of recombinant glutathione-S-transferase (GST)-tagged FGFR1OP. As shown in Fig. 5b, FGFR1OP significantly inhibited the ABL1 kinase activity on WRNIP1 in a dose-dependent manner. We then examined the effect of FGFR1OP overexpression on ABL1-induced cell cycle arrest. We measured the BrdU incorporation ability of A549 cells that were overexpressed either ABL1, or both ABL1 and FGFR1OP, and found that ABL1-induced cell cycle arrest was recovered by overexpression of FGFR1OP (Fig. 5c). These results suggested that FGFR1OP might block phosphorylation of WRNIP1 by ABL1 and play a significant role in pulmonary carcinogenesis.

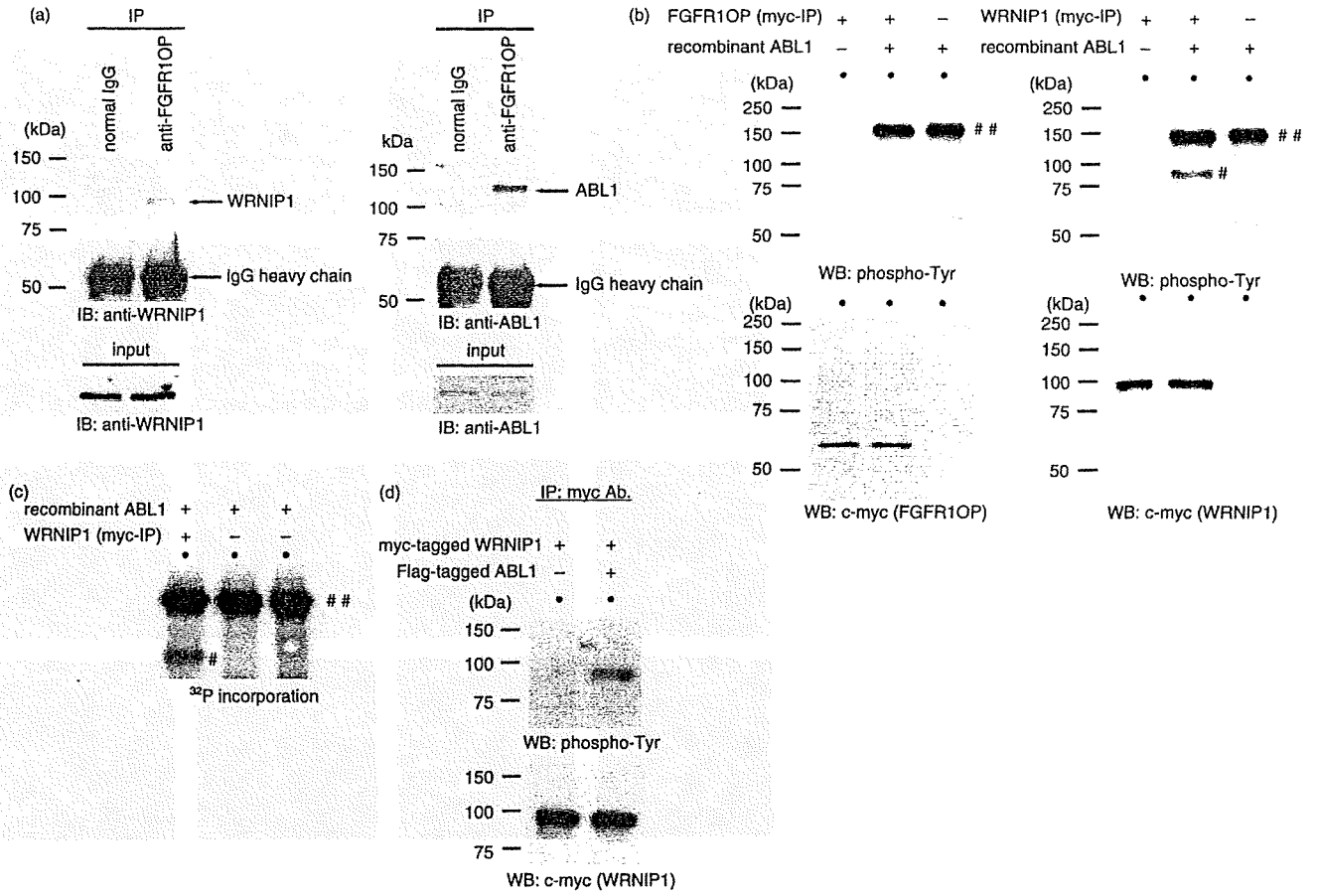

Fig. 4. Interaction of fibroblast growth factor receptor 1 oncogene partner (FGFR1OP) with novel FGFR1OP-binding proteins. (a) Interaction of endogenous FGFR1OP with Werner helicase interacting protein 1 (WRNIP1) and ABL1 in lung cancer cells. Immunoprecipitations were carried out using anti-FGFR1OP antibodies and extracts from LC319 cells. Immunoprecipitates were subjected to western-blot analysis to detect endogenous WRNIP1 (left panels) or ABL1 (right panels). IB, immunoblotting; IP, immunoprecipitation. (b) ABL1 kinase assays, conducted by incubating c-myc-tagged FGFR1OP (left panels; anti-c-myc immunoprecipitates from COS-7 cells transfected with expression plasmids for c-myc-tagged FGFR1OP) or c-myc-tagged WRN1IP (right panels; antic-myc immunoprecipitates from COS-7 cells transfected with expression plasmids for c-myc-tagged WRNIP1) with recombinant ABL1 (as kinase). After the kinase reaction, samples were subjected to western-blot analysis with anti-pan-phosphotyrosine antibodies. The phosphorylated form of WRNIP1 by recombinant ABL1 (#) and the autophosphorylated form of recombinant ABL1 (##) were indicated. (c) c-myc-tagged WRN1IP was incubated with recombinant ABL1 and [γ-^{32}P]-ATP. The reaction samples were analyzed by sodium dodecyl sulfate-polyacrylamide gel electrophoresis (SDS-PAGE) and autoradiography. The phosphorylated form of WRNIP1 by recombinant ABL1 (#) and the autophosphorylated form of recombinant ABL1 (##) were indicated. (d) COS-7 cells were cotransfected with expression plasmids for c-myc-tagged WRNIP1 and expression plasmids for Flag-tagged ABL1 or empty plasmids. The anti-c-myc immunoprecipitates (c-myc-tagged WRNIP1) were subjected to western-blot analysis with anti-pan-phosphotyrosine antibodies.

To further assess whether expression of WRNIP1 plays a role in growth of lung-cancer cells, we then examined the biological significance of the WRNIP1 function in pulmonary carcinogenesis using siRNAs against *WRNIP1* (si-*WRNIP1*-#1 and -#2). Treatment of LC319 cells with siRNA oligonucleotides against WRNIP1 (si-*WRNIP1*-1 or -2) suppressed expression of the endogenous *WRNIP1* in comparison to the control siRNAs (Fig. 5d, left upper panels). In accordance with the reduced expression of *WRNIP1*, LC319 cells showed significant decreases in cell viability and numbers of colonies (Fig. 5d, left lower and right panels). These results strongly supported the possibility that WRNIP1 might also play a significant role in growth and/or survival of lung cancer cells.

Discussion

Molecular-targeted therapies are expected to be highly specific to malignant cells, with minimal risk of adverse reactions due to their well-defined mechanisms of action. Equally desirable prospects are minimally invasive, and highly sensitive and specific new diagnostic methods using selected biomarkers that would adapt readily to clinical settings. As an approach to this goal, we have undertaken a strategy that combines screening of candidate molecules by genome-wide expression analysis with high-throughput screening of loss-of-function effects, using the RNAi technique. In addition, we have been using the tissue-microarray method to analyze hundreds of archived clinical samples for validation of potential target proteins. Using this combined approach, we have shown here that FGFR1OP is frequently overexpressed in clinical lung-cancer samples, and cell lines, and that the gene product plays indispensable roles in the growth and progression of lung-cancer cells.

FGFR1OP protein encodes a 399-amino-acid protein with a LisH domain. LisH motifs in some proteins are reported to be involved in microtubule dynamics and organization, cell migration, and chromosome segmentation.[42,43] A t(6;8)(q27;p11)

doi: 10.1111/j.1349-7006.2007.00610.x

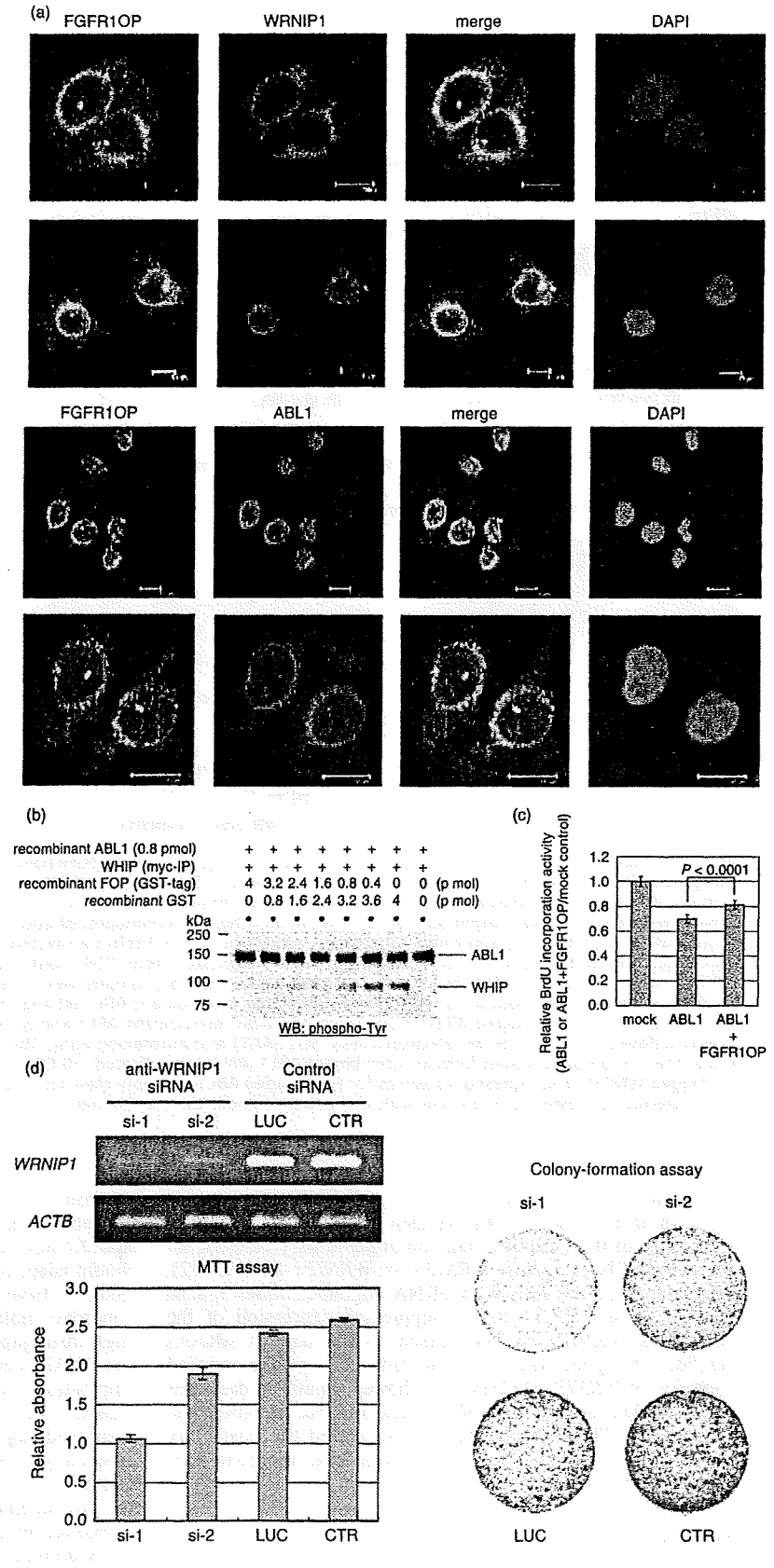

Fig. 5. Significant reduction of ABL1-dependent phosphorylation of Werner helicase interacting protein 1 (WRNIP1) by fibroblast growth factor receptor 1 oncogene partner (FGFR1OP). (a) Immunofluorescence staining of endogenous FGFR1OP and endogenous WRNIP1 in A549 cells. The FGFR1OP-Alexa488 (green), WRNIP1-Alexa594 (red), or cell nuclei (4′6′-diamidino-2-phenylindole dihydrochloride [DAPI]) were visualized. Co-localization of FGFR1OP and WRNIP1 was observed mainly in perinucleus (upper panels). Immunofluorescence staining of endogenous FGFR1OP and endogenous ABL1 in A549 cells. The FGFR1OP-Alexa488 (green), ABL1-Alexa594 (red), or cell nuclei (DAPI) were visualized. Co-localization of FGFR1OP and ABL1 was observed mainly in perinucleus (lower panels). (b) Inhibition of ABL1 kinase activity on WRNIP1 by FGFR1OP. Kinase assays were conducted by incubating c-myc-tagged WRN1IP (as substrate) with recombinant ABL1 (as kinase) in the presence of recombinant GST-tagged FGFR1OP or recombinant GST. After the kinase reaction, samples were subjected to western-blot analysis with antipan-phosphotyrosine antibodies. (c) The effect of FGFR1OP on ABL1-induced cell-cycle arrest was analyzed by BrdU incorporation assay. A549 cells were cotransfected with expression plasmids for Flag-tagged ABL1 and c-myc-tagged FGFR1OP. The cells were allowed to incorporate BrdU for the last 8 h, and its absorbancies were measured. (d) Growth promotive effect of WRNIP1. Inhibition of growth of a lung cancer cell line LC319 by siRNAs against WRNIP1. *Left upper panels,* gene knockdown effect on *WRNIP1* expression in LC319 cells by two si-WRNIP1 (si-WRNIP1-1 and si-WRNIP-2) and two control siRNAs (si-LUC [luciferase] and si-control [CTR]), analyzed by reverse transcription-polymerase chain reaction (RT-PCR). Left lower and right panels, colony formation and MTT assays of LC319 cells transfected with si-WRNIPs or control siRNAs. Columns, relative absorbance of triplicate assays; bars, SD.

chromosomal translocation, fusing FGFR1OP and FGFR1 genes, was found in cases of myeloproliferative disorder.[28–30] The resulting chimeric protein contains the N-terminal leucine-rich region of FGFR1OP protein fused to the catalytic domain of FGFR1. The LisH domain in FGFR1OP-FGFR1 fusion kinase targets the centrosome, activates signaling pathways at this organelle, and sustains continuous entry in the cell cycle.[44] However, since our study by RT-PCR using lung cancer samples detected no expression of chimeric *FGFR1OP-FGFR1*, FGFR1OP-FGFR1 fusion kinase was unlikely to contribute to lung carcinogenesis.

Our treatment of NSCLC cells with specific siRNA to reduce expression of *FGFR1OP* resulted in growth suppression, whereas induction of FGFR1OP promoted the cell growth and increased the cellular invasion activity (Fig. 3). Moreover, clinicopathological evidence through our tissue-microarray experiments demonstrated that NSCLC patients with tumors strongly expressing FGFR1OP showed shorter cancer-specific survival periods than those with negative or weak FGFR1OP expression. The results obtained by *in vitro* and *in vivo* assays strongly suggest that overexpressed FGFR1OP is likely to be an important molecule that may induce a highly malignant phenotype of lung-cancer cells. This is, to our best knowledge, the first study to show the prognostic value of FGFR1OP expression as a cancer biomarker. We should mention also that we found by our genome-wide gene expression profile database the overexpression of FGFR1OP in more than half of bladder cancer, cervical cancer, prostate cancer, renal cell cancer, and osteosarcoma (data not shown). This suggests that overexpression of FGFR1OP might play a significant role in the progression of various types of cancer as well.

We found that FGFR1OP was localized not only in the centrosome, but also in the nucleus, cytoplasm and perinucleus of lung cancer cells (Fig. 1c). These findings suggested that subcellular localization of FGFR1OP might be tightly regulated in a cell-cycle-dependent manner. Interestingly, immunocytochemical analyses revealed colocalization of FGFR1OP with its interacting proteins, WRNIP1 and ABL1, mainly in perinucleus as well as in the nucleus of NSCLC cells at S-G2/M phases (Fig. 5a). The results may suggest the significant role(s) of FGFR1OP through interaction with WRNIP1/ABL1 at this phase during cancer cell cycle progression. WRNIP1 is known to interact with the N-terminal portion of WRN. *Sgs1* and *Mgs1*, the homolog of *WRN* and *WRNIP1*, respectively, were identified in budding yeast.[33,45] Deletion of both *Sgs1* and *Mgs1* increases the rates of terminal G2/M arrest, and then leads to slow growth and shortens life span in yeast cells.[31,34] In fact, our treatment of NSCLC cells with specific siRNA to reduce expression of *WRNIP1* resulted in growth suppression, independently indicating the possible role of WRNIP in cancer cell cycle progression.

On the other hand, the ubiquitously expressed ABL1 is non-receptor tyrosine kinase distributed in the nucleus and cytoplasm.[46] Previous studies have shown that overexpression of ABL1 in Saos-2 cells, which do not express p53 or RB, can activate apoptosis and transient expression of ABL1 weakly induced apoptosis in about 10% of transfected NIH3T3 cells.[47,48] This evidence suggests that ABL1 plays an active role in the cell cycle regulation and death. In this report, we provided evidence that ABL1 could phosphorylate WRNIP1 at tyrosine residues. Interestingly, this enzymatic reaction was likely to be suppressed by FGFR1OP. Although the detailed mechanism of functional interaction among these three proteins remains to be elucidated, targeting this complex might be one of the new approaches to suppress the cancer specific cell signaling that is important for cell proliferation and/or survival.

In summary, we indicated that overexpressed FGFR1OP significantly reduced ABL1-dependent phosphorylation of WRNIP1 and resulted in the cell cycle progression of lung tumors, and that FGFR1OP could be an essential contributor to aggressive features of lung cancers.

Acknowledgment

We thank Wee-Sung Park for her excellent technical contribution to this project.

References

1 Greenlee RT, Hill-Harmon MB, Murray T, Thun M. *Cancer statistics. CA Cancer J Clin* 2001; **51**: 15–36.
2 Sozzi G. Molecular biology of lung cancer. *Eur J Cancer* 2001; **37** (Suppl 7): S63–73.
3 Kelly K, Crowley J, Bunn PA *et al.* Randomized phase III trial of paclitaxel plus carboplatin versus vinorelbine plus cisplatin in the treatment of patients with advanced non-small-cell lung cancer: a Southwest Oncology Group trial. *J Clin Oncol* 2001; **19**: 3210–18.
4 Schiller JH, Harrington D, Belani CP *et al.* Comparison of four chemotherapy regimens for advanced non-small-cell lung cancer. *N Engl J Med* 2002; **346**: 92–8.
5 Kikuchi T, Daigo Y, Katagiri T *et al.* Expression profiles of non-small cell lung cancers on cDNA microarrays: identification of genes for prediction of lymph-node metastasis and sensitivity to anti-cancer drugs. *Oncogene* 2003; **22**: 2192–205.
6 Kikuchi T, Daigo Y, Ishikawa N *et al.* Expression profiles of metastatic brain tumor from lung adenocarcinomas on cDNA microarray. *Int J Oncol* 2006; **28**: 799–805.
7 Kakiuchi S, Daigo Y, Tsunoda T, Yano S, Sone S, Nakamura Y. Genome-wide analysis of organ-preferential metastasis of human small cell lung cancer in mice. *Mol Cancer Res* 2003; **1**: 485–99.
8 Kakiuchi S, Daigo Y, Ishikawa N *et al.* Prediction of sensitivity of advanced non-small cell lung cancers to gefitinib (Iressa, ZD1839). *Hum Mol Genet* 2004; **13**: 3029–43.
9 Ochi K, Daigo Y, Katagiri T *et al.* Prediction of response to neoadjuvant chemotherapy for osteosarcoma by gene-expression profiles. *Int J Oncol* 2004; **24**: 647–55.
10 Yamabuki T, Daigo Y, Kato T *et al.* Genome-wide gene expression profile analysis of esophageal squamous cell carcinomas. *Int J Oncol* 2006 June; **28**: 1375–84.
11 Taniwaki M, Daigo Y, Ishikawa N *et al.* Gene expression profiles of small-cell lung cancers: molecular signatures of lung cancer. *Int J Oncol* 2006; **29**: 567–75.
12 Saito-Hisaminato A, Katagiri T, Kakiuchi S, Nakamura T, Tsunoda T, Nakamura Y. Genome-wide profiling of gene expression in 29 normal human tissues with a cDNA microarray. *DNA Res* 2002; **9**: 35–45.
13 Ochi K, Daigo Y, Katagiri T *et al.* Expression profiles of two types of human knee-joint cartilage. *J Hum Genet* 2003; **48**: 177–82.
14 Suzuki C, Daigo Y, Kikuchi T, Katagiri T, Nakamura Y. Identification of COX17 as a therapeutic target for non-small cell lung cancer. *Cancer Res* 2003; **63**: 7038–41.
15 Suzuki C, Daigo Y, Ishikawa N *et al.* ANLN plays a critical role in human lung carcinogenesis through the activation of RHOA and by involvement in the phosphoinositide 3-kinase/AKT pathway. *Cancer Res* 2005; **65**: 11 314–25.
16 Suzuki C, Takahashi K, Hayama S *et al.* Identification of Myc-associated protein with JmjC domain as a novel therapeutic target oncogene for lung cancer. *Mol Cancer Ther* 2007; **6**: 542–51.
17 Ishikawa N, Daigo Y, Yasui W *et al.* ADAM8 as a novel serological and histochemical marker for lung cancer. *Clin Cancer Res* 2004; **10**: 8363–70.
18 Ishikawa N, Daigo Y, Taniwaki M *et al.* Increases of amphiregulin and transforming growth factor-alpha in serum as predictors of poor response to gefitinib among patients with advanced non-small cell lung cancers. *Cancer Res* 2005; **65**: 9176–84.
19 Ishikawa N, Daigo Y, Takano A *et al.* Characterization of SEZ6L2 cell-surface protein as a novel prognostic marker for lung cancer. *Cancer Sci* 2006; **97**: 737–45.
20 Kato T, Daigo Y, Hayama S *et al.* A novel human tRNA-dihydrouridine synthase involved in pulmonary carcinogenesis. *Cancer Res* 2005; **65**: 5638–46.
21 Kato T, Hayama S, Yamabuki Y *et al.* Increased expression of insulin-like growth factor-II messenger RNA-binding protein 1 is associated with tumor progression in patients with lung cancer. *Clin Cancer Res* 2007; **13**: 434–42.
22 Kato T, Sato N, Hayama S *et al.* Activation of HJURP (Holliday Junction-

doi: 10.1111/j.1349-7006.2007.00610.x

Recognizing Protein) involved in the chromosomal stability and immortality of cancer cells. *Cancer Res* 2007 Sep 6; [Epub ahead of print].
23 Furukawa C, Daigo Y, Ishikawa N *et al.* Plakophilin 3 oncogene as prognostic marker and therapeutic target for lung cancer. *Cancer Res* 2005; **65**: 7102–10.
24 Takahashi K, Furukawa C, Takano A *et al.* The neuromedin u-growth hormone secretagogue receptor 1b/neurotensin receptor 1 oncogenic signaling pathway as a therapeutic target for lung cancer. *Cancer Res* 2006; **66**: 9408–19.
25 Hayama S, Daigo Y, Kato T *et al.* Activation of CDCA1-KNTC2, members of centromere protein complex, involved in pulmonary carcinogenesis. *Cancer Res* 2006; **66**: 10 339–48.
26 Hayama S, Daigo Y, Yamabuki T *et al.* Phosphorylation and activation of cell division cycle associated 8 by aurora kinase B plays a significant role in human lung carcinogenesis. *Cancer Res* 2007; **67**: 4113–22.
27 Yamabuki T, Takano A, Hayama S *et al.* Dickkopf-1 as a Novel Serologic and Prognostic Biomarker for Lung and Esophageal Carcinomas. *Cancer Res* 2007; **67**: 2517–25.
28 Popovici C, Zhang B, Gregoire MJ *et al.* The t (6;8) (q27;p11) translocation in a stem cell myeloproliferative disorder fuses a novel gene, FOP, to fibroblast growth factor receptor 1. *Blood* 1999; **93**: 1381–9.
29 Guasch G, Ollendorff V, Borg JP, Birnbaum D, Pebusque MJ. 8p12 stem cell myeloproliferative disorder: the FOP-fibroblast growth factor receptor 1 fusion protein of the t (6;8) translocation induces cell survival mediated by mitogen–activated protein kinase and phosphatidylinositol 3–kinase/Akt/mTOR pathways. *Mol Cell Biol* 2001; **21**: 8129–42.
30 Guasch G, Delaval B, Arnoulet C *et al.* FOP-FGFR1 tyrosine kinase, the product of a t (6;8) translocation, induces a fatal myeloproliferative disease in mice. *Blood* 2004; **103**: 309–12.
31 Kawabe Y, Branzei D, Hayashi T *et al.* A novel protein interacts with the Werner's syndrome gene product physically and functionally. *J Biol Chem* 2001; **276**: 20 364–9.
32 Kawabe Y, Seki M, Seki T *et al.* Covalent modification of the Werner's syndrome gene product with the ubiquitin-related protein, SUMO-1. *J Biol Chem* 2000; **275**: 20 963–6.
33 Hishida T, Iwasaki H, Ohno T, Morishita T, Shinagawa H. A yeast gene, MGS1, encoding a DNA-dependent AAA(+) ATPase is required to maintain genome stability. *Proc Natl Acad Sci USA* 2001; **98**: 8283–9.
34 Branzei D, Seki M, Onoda F, Enomoto T. The product of Saccharomyces cerevisiae WHIP/MGS1, a gene related to replication factor C genes, interacts functionally with DNA polymerase delta. *Mol Genet Genomics* 2002; **268**: 371–86.
35 Tsurimoto T, Shinozaki A, Yano M, Seki M, Enomoto T. Human Werner helicase interacting protein 1 (WRNIP1) functions as a novel modulator for DNA polymerase delta. *Genes Cells* 2005; **10**: 13–22.
36 Travis WD, Colby TV, Corrin B, Shimosato Y, Brambilla E. *Histological Typing of Lung and Pleural Tumors: World Health Organization International Histological Classification of Tumors*, 3rd edn. Berlin: Springer, 1999.
37 Chin SF, Daigo Y, Huang HE *et al.* A simple and reliable pretreatment protocol facilitates fluorescent *in situ* hybridisation on tissue microarrays of paraffin wax embedded tumour samples. *Mol Pathol* 2003; **56**: 275–9.
38 Callagy G, Cattaneo E, Daigo Y *et al.* Molecular classification of breast carcinomas using tissue microarrays. *Diagn Mol Pathol* 2003; **12**: 27–34.
39 Callagy G, Pharoah P, Chin SF *et al.* Identification and validation of prognostic markers in breast cancer with the complementary use of array-CGH and tissue microarrays. *J Pathol* 2005; **205**: 388–96.
40 Wang JY. Regulation of cell death by the Abl tyrosine kinase. *Oncogene* 2000; **19**: 5643–50.
41 Pendergast AM. The Abl family kinases: mechanisms of regulation and signaling. *Adv Cancer Res* 2002; **85**: 51–100.
42 Emes RD, Ponting CP. A new sequence motif linking lissencephaly, Treacher Collins and oral-facial-digital type 1 syndromes, microtubule dynamics and cell migration. *Hum Mol Genet* 2001; **10**: 2813–20.
43 Umeda M, Nishitani H, Nishimoto T. A novel nuclear protein, Twa1, and Muskelin comprise a complex with RanBPM. *Gene* 2003; **303**: 47–54.
44 Delaval B, Letard S, Lelievre H *et al.* Oncogenic tyrosine kinase of malignant hemopathy targets the centrosome. *Cancer Res* 2005; **65**: 7231–40.
45 Gangloff S, McDonald JP, Bendixen C, Arthur L, Rothstein R. The yeast type I topoisomerase Top3 interacts with Sgs1, a DNA helicase homolog: a potential eukaryotic reverse gyrase. *Mol Cell Biol* 1994; **14**: 8391–8.
46 Wen ST, Jackson PK, Van Etten RA. The cytostatic function of c-Abl is controlled by multiple nuclear localization signals and requires the p53 and Rb tumor suppressor gene products. *EMBO J* 1996; **15**: 1583–95.
47 Theis S, Roemer K. c-Abl tyrosine kinase can mediate tumor cell apoptosis independently of the Rb and p53 tumor suppressors. *Oncogene* 1998; **17**: 557–64.
48 Cong F, Goff SP. c-Abl-induced apoptosis, but not cell cycle arrest, requires mitogen-activated protein kinase kinase 6 activation. *Proc Natl Acad Sci USA* 1999; **96**: 13 819–24.

Increased expression of h-prune is associated with tumor progression and poor survival in gastric cancer

Naohide Oue,[1] Kazuhiro Yoshida,[2] Tsuyoshi Noguchi,[3] Kazuhiro Sentani,[1] Akira Kikuchi[4] and Wataru Yasui[1,5]

[1]Department of Molecular Pathology, Hiroshima University Graduate School of Biomedical Sciences, Hiroshima 734-8551; [2]Department of Surgical Oncology, Research Institute for Radiation Biology and Medicine, Hiroshima University, Hiroshima 734-8551; [3]Department of Oncological Science (Surgery II), Oita University Faculty of Medicine, Oita 879-5593; [4]Department of Biochemistry, Hiroshima University Graduate School of Biomedical Sciences, Hiroshima 734-8551, Japan

(Received February 14, 2007/Revised March 28, 2007/Accepted April 3, 2007/Online publication May 23, 2007)

The human homolog of the *Drosophila* prune protein (from *PRUNE*, which encodes h-prune), which interacts with glycogen synthase kinase 3, promotes cellular motility. H-prune also interacts with nm23-H1, a suppressor of cancer metastasis. It has been reported that stimulation of cellular motility by h-prune is enhanced by its interaction with nm23-H1 in breast cancer cells. In the present study, we examined the expression of h-prune and nm23-H1 during tumor progression in gastric cancer (GC). *PRUNE* mRNA was overexpressed in 12 (32%) of 38 GC cases by quantitative reverse transcription–polymerase chain reaction. *PRUNE* mRNA levels correlated significantly with advanced T grade, N grade and tumor stage. Immunohistochemical analysis revealed that 43 (30%) of 143 GC cases were positive for h-prune, and h-prune-positive GC cases showed more advanced T grade, N grade and tumor stage than h-prune-negative GC cases. One hundred and twenty-four (87%) of 143 GC cases were positive for nm23-H1, and nm23-H1 was expressed in almost all (42 cases, 98%) h-prune-positive GC cases. Many GC cases positive for both h-prune and nm23-H1 showed more advanced T grade, N grade and tumor stage than other type GC cases. Patients with h-prune-positive GC had a significantly worse survival rate than patients with h-prune-negative GC. These findings indicate that overexpression of h-prune is associated with tumor progression and aggressiveness of GC. nm23-H1 may enhance motility of cancer cells by interacting with h-prune. (*Cancer Sci* 2007; 98: 1198–1205)

According to the World Health Organization, gastric cancer (GC) is the fourth most common malignancy worldwide, with approximately 870 000 new cases occurring yearly. Mortality due to GC is second only to that due to lung cancer.[1] Advances in diagnostic tools and treatment have led to excellent long-term survival for early GC.[2] However, despite improvements in diagnostic and therapeutic strategies, the prognosis of advanced GC with extensive invasion and metastasis remains poor. Several discrete steps can be discerned in the biological cascade of metastasis: loss of cellular adhesion, increased motility and invasiveness, entry and survival in the circulation, exit into new tissue, and eventual colonization of a distant site.[3] Several molecules associated with invasion and metastasis have been identified,[4,5] but these molecules cannot completely explain the mechanism of each step of metastasis. In addition, many genes have been analyzed to understand the molecular basis of GC,[6,7] but only a few with frequent alterations have been identified so far.

Previously, we identified the human homolog of *Drosophila* prune protein (*PRUNE*, which encodes h-prune) as a glycogen synthase kinase 3 (GSK-3)-binding protein.[8] GSK-3 inhibitors or small interfering RNA (siRNA) for GSK-3 and h-prune inhibit cell motility. H-prune is localized to focal adhesions, and the siRNA for GSK-3 or h-prune delays the disassembly of paxillin. Tyrosine phosphorylation of focal adhesion kinase (FAK) and activation of Rac are suppressed in GSK-3 or h-prune knock-down cells.[8] These results suggest that GSK-3 and h-prune act cooperatively to regulate cellular motility. In fact, overexpression of h-prune has been reported in breast cancers and is also associated with high metastatic potential.[9] In our previous study, overexpression of h-prune was correlated with T grade (depth of invasion), N grade (degree of lymph node metastasis), and tumor stage in colorectal cancers (CRC).[8]

H-prune has phosphodiesterase (PDE) activity, with a preferential affinity for cAMP over cGMP as substrate.[9] PDE are a diverse superfamily of molecules that catalyze the hydrolysis of 3′,5′-cyclic nucleotides to their corresponding nucleoside 5′-monophosphates.[10] H-prune PDE activity is involved in cellular motility,[9] and h-prune also interacts with nm23-H1 (*NME1*, which encodes nm23-H1),[11] a known suppressor of cancer metastasis.[12] H-prune and nm23-H1 proteins partially colocalize in the cytoplasm.[11] It has been suggested that overexpression of h-prune inhibits the antimetastasis function of nm23-H1 during the metastatic process.[9,13] Several studies have suggested an association between reduced expression of nm23 mRNA or protein and increasing metastatic activity, resulting in poorer prognosis in breast cancers,[14] malignant melanomas[15] and hepatocellular carcinomas.[16] In contrast, in GC and CRC, overexpression of nm23-H1 has been reported.[17,18] High nm23-H1 expression has been shown to correlate with tumor progression and poor prognosis of GC.[19]

Taken together, the currently available data suggest that analysis of h-prune is necessary to clarify the association between expression of nm23-H1 and metastatic potential. Correlation between high nm23-H1 expression and metastatic potential in GC may be due to overexpression of h-prune. However, expression of h-prune has not been investigated in GC. In the present study, we examined the expression and distribution of both h-prune and nm23-H1 in human GC by immunohistochemistry and reverse transcription–polymerase chain reaction (RT-PCR).

Materials and Methods

Tissue samples. In a retrospective study design, 181 primary tumors were collected from patients diagnosed with GC who underwent surgery between 1991 and 2001 at the Department of Surgical Oncology, Hiroshima University Hospital (Hiroshima, Japan). All patients underwent curative resection. Only patients without preoperative radiotherapy or chemotherapy and without clinical evidence for distant metastasis were enrolled in the study.

For quantitative RT-PCR, 38 GC samples and corresponding non-neoplastic mucosa samples were used. The samples were obtained during surgery at Hiroshima University Hospital. We confirmed microscopically that the tumor specimens were

[5]To whom correspondence should be addressed. E-mail: wyasui@hiroshima-u.ac.jp

doi: 10.1111/j.1349-7006.2007.00515.x

predominantly cancer tissue (>50% on a nuclear basis). Samples were frozen immediately in liquid nitrogen and stored at −80°C until use.

For immunohistochemical analysis, we used archival formalin-fixed, paraffin-embedded tissues from 143 patients who had undergone surgical excision for GC. Fifty-nine of the 143 patients had early GC, and 84 had advanced GC. Early GC is limited to the mucosa or the mucosa and submucosa, regardless of nodal status.[2] Advanced GC is a tumor that has invaded beyond the muscularis propria. Information on patient prognosis was available for 84 GC cases. Because information on postoperative chemotherapy was not available, postoperative chemotherapeutic backgrounds were not involved in the prognostic analysis.

Tumor staging was carried out according to the tumor–node–metastasis (TNM) stage grouping.[20] Histological classification of GC was carried out according to the Lauren classification system.[21] Because written informed consent was not obtained, for strict privacy protection, identifying information for all samples was removed before analysis; this procedure is in accordance with Ethical Guidelines for Human Genome/Gene Research enacted by the Japanese Government and approved by the Ethical Review Committee of the Hiroshima University School of Medicine.

Quantitative RT-PCR analysis. Total RNA was extracted with an RNeasy Mini Kit (Qiagen, Valencia, CA, USA), and 1 μg of total RNA was converted to cDNA with a First Strand cDNA Synthesis Kit (Amersham Biosciences, Piscataway, NJ, USA). Quantitation of *PRUNE* mRNA levels in human tissue samples was done by real-time fluorescence detection as described previously.[22] *PRUNE* primer sequences were 5′-GAA GTC CTG GAA CGC TCC C-3′ and 5′-GGT TAG GGT GGG TAC TTG AGG C-3′. PCR was carried out using a SYBR Green PCR Core Reagents Kit (Applied Biosystems, Foster City, CA, USA). Real-time detection of the emission intensity of SYBR green bound to double-stranded DNA was done with an ABI PRISM 7700 Sequence Detection System (Applied Biosystems) as described previously.[23] *ACTB*-specific PCR products were amplified from the same RNA samples and served as internal controls.

Immunohistochemistry. A Dako LSAB kit (Dako, Carpenteria, CA, USA) was used for immunohistochemical analysis. In brief, sections were pretreated by microwaving in citrate buffer for 30 min to retrieve antigenicity. After peroxidase activity was blocked with 3% H_2O_2–methanol for 10 min, sections were incubated with normal goat serum (Dako) for 20 min to block non-specific antibody binding sites. Sections were incubated with rabbit polyclonal antih-prune (diluted 1:50, antih-prune antibody was raised in our laboratory)[8] and rabbit polyclonal antinm23-H1 (1:20, Santa Cruz Biotechnology, Santa Cruz, CA, USA). The specificity of the h-prune antibody has been characterized in detail.[8] Sections were incubated with primary antibody for 1 h at 25°C, followed by incubations with biotinylated antirabbit IgG and peroxidase-labeled streptavidin for 10 min each. Staining was completed with a 10-min incubation with the substrate–chromogen solution. The sections were counterstained with 0.1% hematoxylin. The percentage of stained cancer cells was evaluated for each antibody.

Statistical methods. Correlations between clinicopathological parameters and h-prune or nm23-H1 expression were analyzed by Fisher's exact test. Kaplan–Meier survival curves were constructed for h-prune- or nm23-H1-positive and h-prune- or nm23-H1-negative patients. Survival rates were compared between h-prune- or nm23-H1-positive and h-prune- or nm23-H1-negative groups. Differences between survival curves were tested for statistical significance using the log-rank test.[24] Cox proportional hazards multivariate model was used to examine the association of clinical and pathological factors and the expression of h-prune with survival. A *P*-value of less than 0.05 was considered statistically significant.

Results

mRNA expression of *PRUNE* in GC. Expression of *PRUNE* mRNA was analyzed by quantitative RT-PCR of RNA from 38 GC samples and corresponding non-neoplastic mucosa samples. We calculated the ratio of *PRUNE* mRNA levels between GC tissue (T) and corresponding non-neoplastic mucosa (N). When a T/N ratio > two-fold was considered to represent overexpression, *PRUNE* was overexpressed in 12 (32%) of the 38 GC samples. As shown in Fig. 1, *PRUNE* levels were significantly higher in T3/4 cases than in T1/2 cases ($P = 0.0156$; Mann–Whitney *U*-test). Moreover, *PRUNE* levels correlated significantly with N status ($P = 0.0122$; Mann–Whitney *U*-test) and tumor stage ($P = 0.0127$; Mann–Whitney *U*-test). There was no clear tendency between *PRUNE* level and histological type.

Immunohistochemical analysis of h-prune in GC. We next investigated the expression and distribution of h-prune by immunohistochemistry of 143 GC tissue samples. In corresponding non-neoplastic gastric mucosa, only weak or no staining of h-prune was observed in epithelial and stromal cells (Fig. 2a,b). However, GC tissue showed stronger, more extensive staining than corresponding non-neoplastic mucosa. In 14 (10%) of the 143 GC cases, h-prune-positive tumor cells were restricted to the invasive front (Fig. 2a,c,d). In these cases, less than 50% of tumor cells were stained. However, in the majority of GC cases containing h-prune-positive tumor cells, more than 50% of the tumor cells showed cytoplasmic staining for h-prune (43 of 143 GC cases). In these GC cases, h-prune-positive tumor cells were observed at the invasive front in addition to the central part of the tumors. The remaining cases showed 10–50% immunopositive tumor cells and h-prune staining was not observed at the invasive front. H-prune was detected in the cytoplasm of tumor cells in intestinal-type (Fig. 2e) and diffuse-type GC (Fig. 2f,g). We next analyzed the relationship between h-prune expression and clinicopathological characteristics. Several previous studies have indicated that observation of the invasive front is important in the analysis of tumor cells, because it reflects the invasive potential of those cells. To investigate the significance of restricted h-prune staining at the invasive front, the relationship between h-prune staining and clinicopathological characteristics was examined in GC cases in which less than 50% of tumor cells were stained. In these cases, GC cases in which h-prune-positive tumor cells were restricted to the invasive front showed more advanced T grade ($P = 0.0083$, Fisher's exact test) than those in which h-prune-positive tumor cells were not restricted to the invasive front (Table 1). GC cases in which h-prune-positive tumor cells were restricted to the invasive front did not show advanced N grade or tumor stage (Table 1). In contrast, among all of the cases we studied, GC cases in which more than 50% of tumor cells were stained showed more advanced T grade ($P = 0.0158$, Fisher's exact test), N grade ($P = 0.0035$, Fisher's exact test) and tumor stage ($P = 0.0466$, Fisher's exact test) than those in which less than 50% of tumor cells were stained (Table 1). Therefore, when more than 50% of tumor cells were stained, the immunostaining was considered positive for h-prune.

Association between h-prune and nm23-H1 expression. Because it has been suggested that overexpression of h-prune in breast cancer inhibits the antimetastasis function of nm23-H1 during metastasis,[9,13] we also carried out immunohistochemical analysis of nm23-H1 in the same 143 GC cases. Consistent with previous reports,[19] strong cytoplasmic staining of nm23-H1 was observed in tumor cells. In corresponding non-neoplastic mucosa, weak staining of nm23-H1 was observed. In the present study, to compare the h-prune staining pattern with the

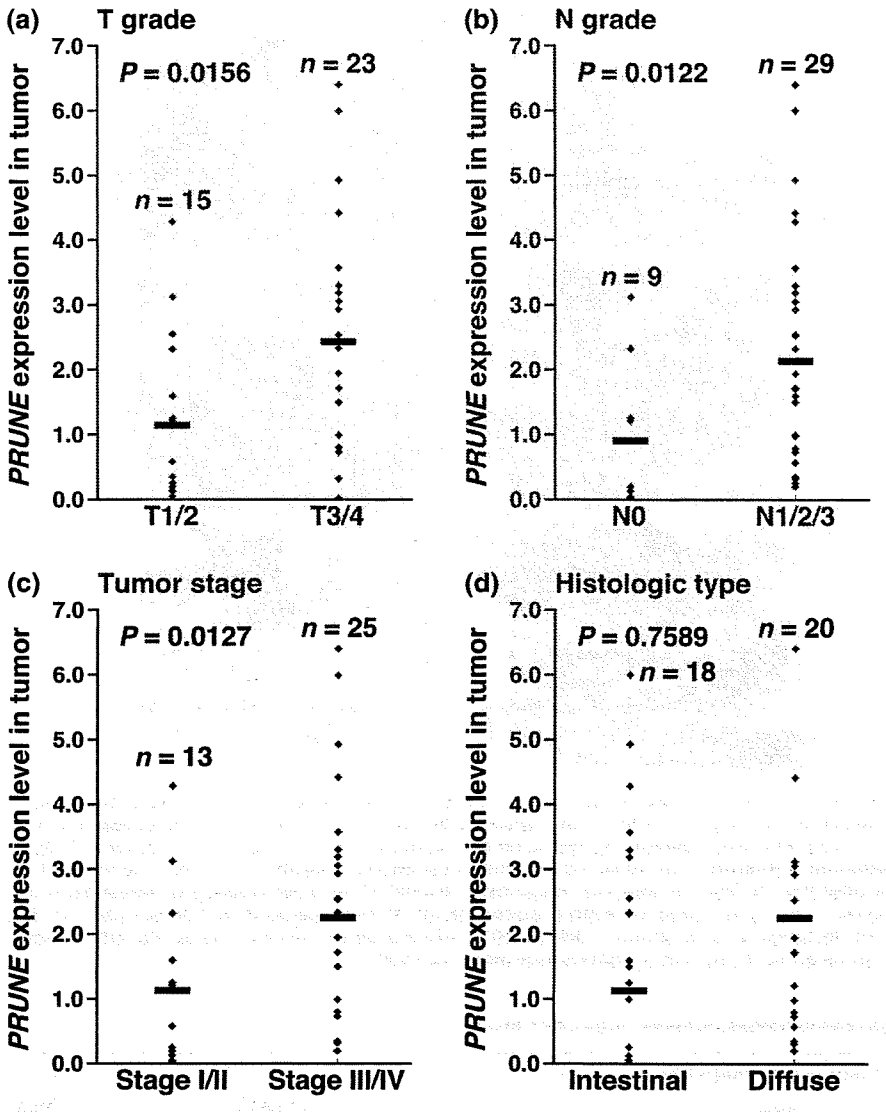

Fig. 1. Expression of PRUNE mRNA in gastric cancer tissues. Each point represents the levels of PRUNE mRNA in an individual specimen. Horizontal bar represents the mean PRUNE mRNA expression level. (a) PRUNE mRNA expression levels were significantly higher in T3/4 cases than in T1/2 cases ($P = 0.0156$; Mann–Whitney *U*-test). (b) The PRUNE mRNA expression levels were significantly higher in N1/2/3 cases than in N0 cases ($P = 0.0122$; Mann–Whitney *U*-test). (c) The PRUNE mRNA expression levels were significantly higher in stage III/IV cases than in stage I/II cases ($P = 0.0127$; Mann–Whitney *U*-test). (d) There was no clear association between PRUNE mRNA expression level and histological type.

nm23-H1 staining pattern, the same cut-off point for nm23-H1 and h-prune immunostaining was set. When more than 50% of tumor cells were stained, the immunostaining was considered positive for nm23-H1. In total, 124 (87%) of 143 GC cases were positive for nm23-H1. The h-prune staining pattern was then compared with the nm23-H1 staining pattern. Of 43 h-prune-positive GC cases, 42 (98%) were positive for nm23-H1, and in these 42 GC cases there was a tendency for h-prune and nm23-H1 to be expressed in the same tumor cells (Fig. 3a,b). All 18 GC cases that were negative for both h-prune and nm23-H1 were signet ring cell carcinoma. In contrast, the majority (82 of 143 GC cases, 57%) of cases were positive for nm23-H1 but not h-prune (Fig. 3c,d). The frequency of nm23-H1 expression in h-prune-positive GC cases (42 of 43 cases, 98%) was significantly higher than that in h-prune-negative GC cases (82 of 100 cases, 82%, $P = 0.0134$, Fisher's exact test) (Table 2).

We next analyzed the relationship between nm23-H1 expression and clinicopathological characteristics. Expression of nm23-H1 was not correlated with age, sex, T grade, N grade or tumor stage (Table 3). As reported previously,[19] expression of nm23-H1 was observed more frequently in intestinal-type GC (79 of 85 cases, 93%) than in diffuse-type GC (45 of 58 cases, 78%, $P = 0.0113$, Fisher's exact test) (Table 3). It has been reported that in the majority of nm23-H1-positive tumors, more than 75% of the tumor cells contained a homogeneous cytoplasmic pattern for nm23-H1.[19] GC cases containing more than 75% of nm23-H1-positive tumor cells were found in 113 of 143 GC cases. GC cases containing more than 75% of nm23-H1-positive tumor cells did not show advanced T grade, N grade or tumor stage (data not shown). Among the nm23-H1-positive GC cases, h-prune-positive GC cases showed advanced T grade ($P = 0.0341$, Fisher's exact test), N grade ($P = 0.0083$, Fisher's exact test) and tumor stage ($P = 0.0371$, Fisher's exact test) more frequently than h-prune-negative GC cases (Fig. 4a–c). In contrast, among h-prune-negative GC cases there was no statistically significant correlation between nm23-H1 positivity and T grade, N grade or tumor stage (Fig. 4a–c).

We also examined the relationship between survival and expression of h-prune and nm23-H1 in GC ($n = 84$). On univariate analysis, T grade ($P < 0.0001$, log-rank test), N grade ($P = 0.0474$, log-rank test), tumor stage ($P = 0.0001$, log-rank test) and h-prune expression ($P < 0.0001$, log-rank test) (Fig. 4d) were significant prognostic factors of survival in patients with GC, whereas age, sex, histological type and nm23-H1 expression (Fig. 4e) were not correlated with survival. Next, Cox proportional hazards multivariate model was used to examine the association of clinicopathological factors and the expression of h-prune with survival. Multivariate analysis indicated that T grade, N grade, tumor stage and h-prune expression were independent predictors of survival in patients with GC (Table 4).

doi: 10.1111/j.1349-7006.2007.00515.x

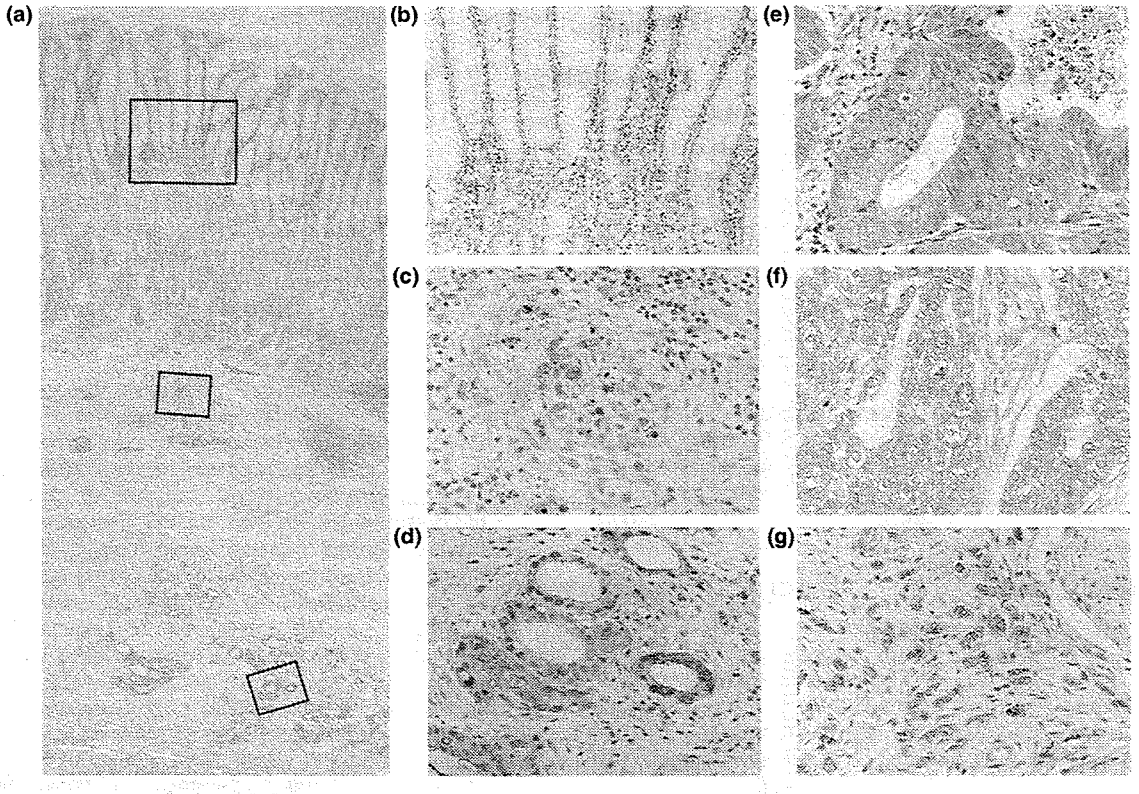

Fig. 2. Immunohistochemical analysis of h-prune in gastric cancer (GC) tissues. (a) GC case in which h-prune expression was strong at the invasive front (original magnification, ×40). (b,c,d) High magnification images of the fields indicated by boxes in panel (a). (b) In corresponding non-neoplastic gastric mucosa, only weak or no staining of h-prune was observed in epithelial and stromal cells (original magnification, ×100). (c) In the superficial layer of GC tissue, only weak or no staining of h-prune was observed (original magnification, ×400). (d) In the invasive front of GC tissue, strong cytoplasmic staining of h-prune was observed in GC cells (original magnification, ×400). (e) H-prune-positive intestinal-type GC. Strong cytoplasmic staining of h-prune was observed in GC cells (original magnification, ×400). (f) H-prune-positive diffuse-type GC. Strong cytoplasmic staining of h-prune was observed in GC cells (original magnification, ×400). (g) H-prune-positive diffuse-type GC (so-called scirrhous-type GC). Strong cytoplasmic staining of h-prune was observed in GC cells (original magnification, ×400).

Table 1. Association of h-prune expression with clinicopathologic features of gastric cancer

Feature	H-prune expression (%)			*P*-value†	*P*-value‡
	Positive	Invasion front positive	Negative		
Age (years)					
>65	20 (25%)	6 (7%)	55	0.1504	0.1410
≤65	23 (37%)	8 (13%)	31		
Sex					
Male	25 (27%)	10 (11%)	57	0.7703	0.3442
Female	18 (35%)	4 (8%)	29		
T grade§					
T1	11 (19%)	2 (3%)	46	0.0083	0.0158
T2/3/4	32 (38%)	12 (14%)	40		
N grade§					
N0	16 (20%)	6 (8%)	58	0.1305	0.0035
N1/2/3	27 (43%)	8 (13%)	28		
Stage§					
Stage I/II	25 (25%)	8 (8%)	68	0.0944	0.0466
Stage III/IV	18 (43%)	6 (14%)	18		
Histological type¶					
Intestinal	22 (26%)	9 (11%)	54	1.0000	0.1988
Diffuse	21 (36%)	5 (9%)	32		

†Invasion front positive versus negative. Statistical significance was determined with Fisher's exact test. ‡Positive versus invasion front-positive plus-negative. Statistical significance was determined with Fisher's exact test. §Stage was classified according to the criteria of the International Union Against Cancer TNM classification of malignant tumors.[20] ¶Histology was classified according to the criteria of Lauren.

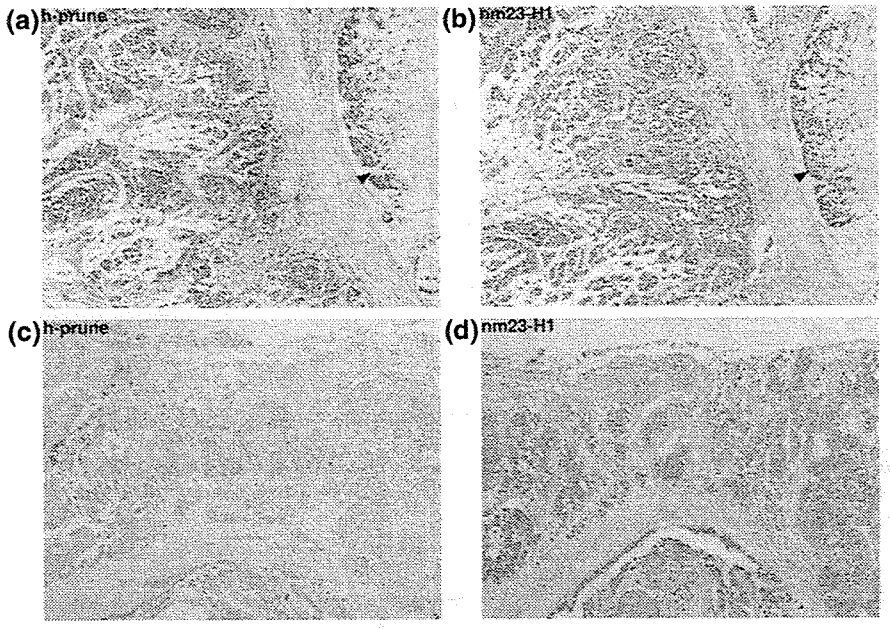

Fig. 3. Expression and distribution of h-prune and nm23-H1 in gastric cancer (GC) tissues. (a) Immunohistochemistry of h-prune in h-prune-positive GC case. Staining for h-prune was observed in diffuse-type GC cells but not in signet ring cell carcinoma components (arrowhead) (original magnification, ×100). (b) Immunohistochemistry of nm23-H1 in the same GC case as in panel (a). H-prune and nm23-H1 tended to be located in the same GC cells (original magnification, ×100). (c) Immunohistochemistry of h-prune in h-prune-negative GC case (original magnification, ×100). (d) Immunohistochemistry of nm23-H1 in the same GC case as in panel (c). Staining of nm23-H1 was observed in GC cells (original magnification, ×100).

Table 2. Distribution of h-prune and nm23-H1 expression in gastric cancer

H-prune expression	nm23-H1 expression		*P*-value†
	Positive	Negative	
Positive	42 (98%)	1	0.0134
Negative	82 (82%)	18	

†Statistical significance was determined with Fisher's exact test.

Table 3. Association of nm23-H1 expression with clinicopathologic features of gastric cancer

Feature	nm23-H1 expression (%)		*P*-value†
	Positive	Negative	
Age (years)			
>65	70 (86%)	11	1.0000
≤65	54 (87%)	8	
Sex			
Male	80 (87%)	12	1.0000
Female	44 (86%)	7	
T grade‡			
T1	49 (83%)	10	0.3220
T2/3/4	75 (89%)	9	
N grade‡			
N0	68 (85%)	12	0.6219
N1/2/3	56 (89%)	7	
Stage‡			
Stage I/II	88 (87%)	13	0.7926
Stage III/IV	36 (86%)	6	
Histological type§			
Intestinal	79 (93%)	6	0.0113
Diffuse	45 (78%)	13	

†Statistical significance was determined with Fisher's exact test. ‡Stage was classified according to the criteria of the International Union Against Cancer TNM classification of malignant tumors.[20] §Histology was classified according to the criteria of Lauren.

Discussion

Metastasis fundamentally involves the movement of cells from one site to another. The molecular mechanisms that underlie cell migration involve dynamic cytoskeletal changes, cell–matrix interactions, localized proteolysis, actin–myosin contractions and focal contact disassembly.[25] We reported previously that h-prune is localized to focal adhesions and that knockdown of h-prune inhibits cell motility. Suppression of tyrosine phosphorylation of FAK and activation of Rac are involved in inhibition of cell motility.[8] In the present study, overexpression of *PRUNE* mRNA was observed in 32% of cases by quantitative RT-PCR analysis, and cytoplasmic staining of h-prune protein was observed in 30% of cases by immunohistochemistry in GC tissue samples. Expression of h-prune was correlated with T grade, N grade and tumor stage. In addition, patients with h-prune-positive GC had a significantly worse survival rate than patients with h-prune-negative GC. Taken together, these results suggest that extensive expression of h-prune contributes to the malignant behavior of GC, possibly by promoting cancer cell motility. H-prune may be a good marker of poor survival of GC.

It is generally accepted that cancer progresses as a disease of genetically heterogeneous cell populations. In the present study, there were several cases in which h-prune-positive tumor cells were restricted to the invasive front. Among GC cases in which less than 50% of tumor cells were stained, GC cases in which h-prune-positive tumor cells were restricted to the invasive front showed more advanced T grade than those in which h-prune-positive tumor cells were not restricted to the invasive front; however, these GC cases comprised only 10% of 143 GC cases, and did not show advanced N grade or tumor stage, suggesting that expression of h-prune may represent tumor invasiveness, especially local invasiveness. Observation of the invasive front is important in the analysis of tumor cells, because it reflects the invasive potential of tumor cells. It has been reported that expression of matrilysin in the invasive front is a promising biomarker predicting nodal metastasis of colorectal cancers.[26] Overexpression of heparanase at the invasive front has been reported in GC, and high expression of heparanase is a strong predictor of poor survival.[27] These results indicate that the proteolytic degradation of extracellular matrix by these molecules is one of the most important mechanisms in tumor progression, and the proteolytic degradation occurs at the invasive front.

doi: 10.1111/j.1349-7006.2007.00515.x

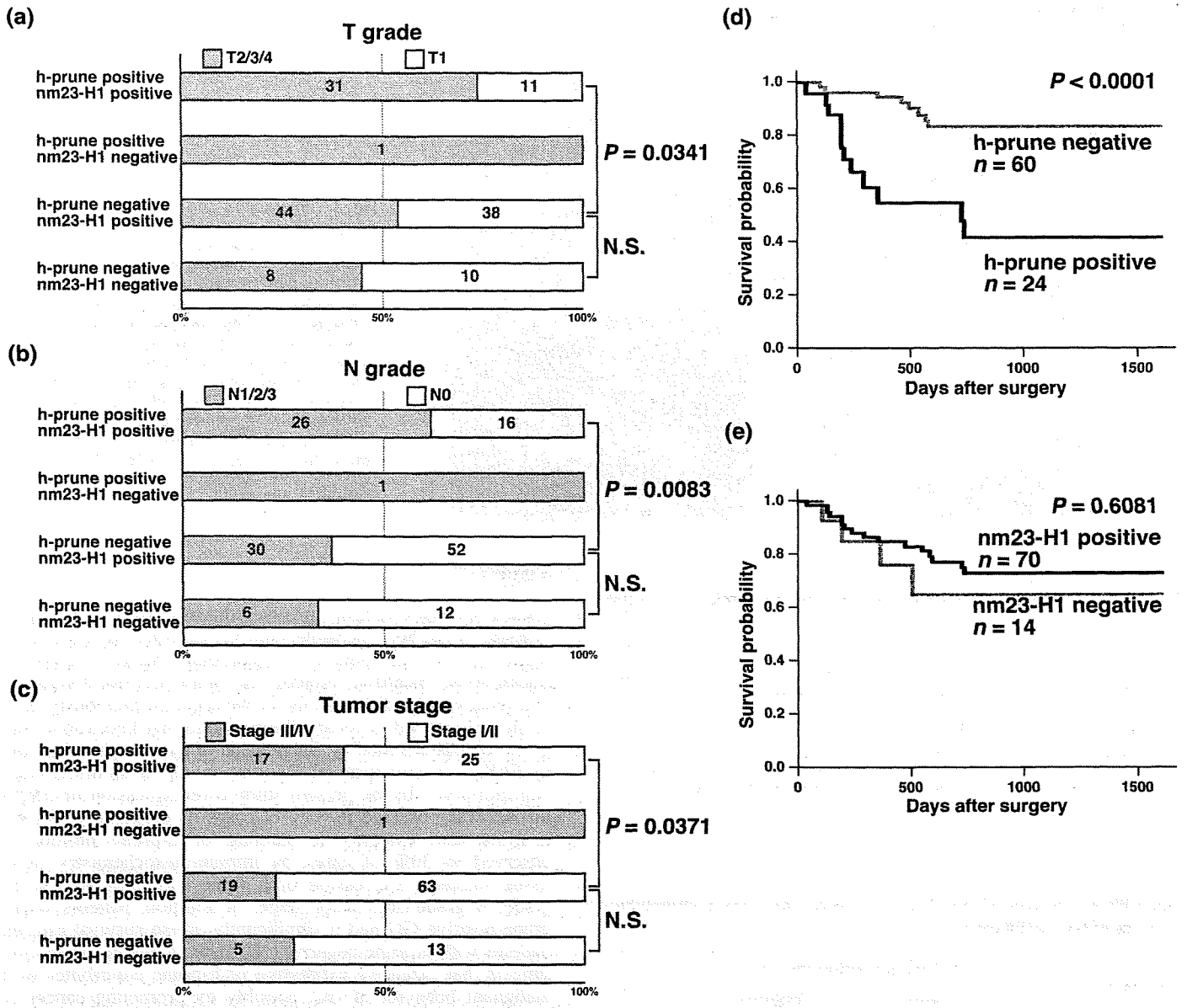

Fig. 4. Correlation of h-prune and nm23-H1 expression with clinicopathologic features. Many gastric cancer (GC) cases positive for both h-prune and nm23-H1 showed advanced (a) T grade, (b) N grade and (c) tumor stage. There were no clear differences between h-prune-negative/nm23-H1-positive GC cases and h-prune-negative/nm23-H1-negative GC cases. There was only h-prune-positive/nm23-H1-negative GC among 143 GC cases. (d) The survival of patients with h-prune-positive GC was significantly worse in 84 patients with GC ($P < 0.0001$, log-rank test). (e) There was no statistical difference between the survival rate of patients with nm23-H1-positive GC and that of patients with nm23-H1-negative GC ($P = 0.6081$, log-rank test).

Because h-prune promotes cell motility, expression of h-prune at the invasive front may partly contribute to the malignant behavior of GC, such as local invasiveness.

The mechanism of regulation of h-prune expression is still unknown. In the present study, overexpression of *PRUNE* mRNA was observed in 32% by quantitative RT-PCR analysis, and h-prune-positive GC cases were found in 30% by immunohistochemistry. Because GC samples analyzed by quantitative RT-PCR were different from those analyzed by immunohistochemistry, we could not compare *PRUNE* mRNA levels with h-prune protein levels. However, these findings suggest that overexpression of *PRUNE* occurs at the transcriptional or mRNA level in GC. *PRUNE* amplification and overexpression have been reported in certain sarcomas and breast cancers.[13] *PRUNE* is located on chromosome 1q21.3, and gains of 1q21.1-21.2 and 1q21.3 have been reported in GC.[28] Amplification of the *PRUNE* gene may be involved in overexpression of h-prune in GC cases. The main cause of peptic ulceration is *Helicobacter pylori*, and *H. pylori* is the strongest risk factor for the development of distal GC.[29,30] Because stimulation of matrilysin by *H. pylori* has been reported,[31] induction of h-prune by *H. pylori* should be examined in the near future.

In the present study, immunohistochemical analysis of GC tissues revealed that almost all h-prune-positive GC cases (98%) also expressed nm23-H1. Expression of nm23-H1 was found in both early- and late-stage GC, whereas expression of h-prune was detected mainly in late-stage tumors. In nm23-H1-positive GC cases, h-prune-positive GC cells may develop in accordance with tumor progression. In GC cases positive for both h-prune and nm23-H1, intratumoral distribution of h-prune-positive tumor cells and nm23-H1-positive tumor cells was similar, and many of these GC cases showed advanced T grade, N grade and

Table 4. Multivariate analysis of factors influencing survival

Factor	Hazard ratio	95% CI	χ^2	*P*-value
T grade†				
T1	1	Reference	7.42	0.0064
T2/3/4	18.99	2.28–157.86		
N grade†				
N0	1	Reference	5.57	0.0182
N1/2/3	8.24	1.43–47.46		
Stage†				
Stage I/II	1	Reference	5.71	0.0168
Stage III/IV	6.42	1.39–29.43		
H-prune expression				
Negative	1	Reference	8.18	0.0043
Positive	4.87	1.63–14.48		

†Stage was classified according to the criteria of the International Union Against Cancer TNM classification of malignant tumors.[20]

tumor stage. Because the PDE activity of h-prune, which is involved in cellular motility, is enhanced by the interaction with nm23-H1,[9] expression of both proteins may confer cellular motility to GC cells. Among h-prune-negative GC cases, there were no clear differences between nm23-H1 positivity and clinical characteristics, suggesting that expression of only nm23-H1 does not influence progression of GC. Although there was no impact of nm23-H1 expression on patient survival in the present study, it has been reported that high nm23-H1 expression correlates with tumor progression and poor prognosis.[9] Expression of nm23-H1 may enhance the PDE activity of h-prune but may not have antimetastatic activity. All 18 GC cases negative for both h-prune and nm23-H1 were signet ring cell carcinoma. Several reports have indicated that the prognosis of patients with signet ring cell carcinoma is relatively favorable in the early stages and poor in advanced stages compared with other histological types of GC.[32] In fact, of 18 signet ring cell carcinoma cases, 12 cases showed stage I and the prognosis of patients with these GC was favorable.

Epigenetic changes, such as DNA methylation of CpG islands, are detected commonly in human cancers. Hypermethylation of CpG islands is associated with silencing of many genes, especially defective tumor-related genes, and has been proposed as an alternative way to inactivate tumor-related genes in human cancers.[33] GC show the CpG island methylator phenotype (CIMP).[34,35] CIMP-positive GC also tend to show DNA methylation of the $p16^{INK4a}$,[34] *hMLH1*[6] and *RIZ*[6] genes, suggesting that CIMP is an important pathway involved in stomach carcinogenesis. Because DNA methylation inhibitors such as 5-aza-2′-deoxycytidine have been shown to increase nm23-H1 expression in breast cancer cells,[36] h-prune or nm23-H1 expression may be associated with CIMP.

Is h-prune a good therapeutic target for GC? Previous data indicated that dipyridamole, an antiplatelet aggregation drug, inhibits h-prune PDE activity and cellular motility in a breast cancer cell line.[9] In the SW480 CRC cell line, knockdown of h-prune decreased cell motility.[8] These results suggest that inhibition of h-prune may be useful for the prevention or treatment of metastasis. However, because h-prune is expressed ubiquitously in normal human adult tissues,[11] inhibitors of h-prune, such as dipyridamole, may have severe adverse effects. However, it is known that components of the blood-clotting pathway contribute to metastasis by trapping tumor cells in capillaries or by facilitating adhesion of tumor cells to capillary walls. Anti-platelet aggregation drugs may interfere with this step in the metastatic process. In fact, several studies have indicated that the formation of metastatic tumors could be inhibited by antiplatelet aggregation drugs (reviewed by Hejna *et al.*[37]). In GC, combined chemotherapy with dipyridamole with adriamycin and 5-fluorouracil appears to be safe and may be useful clinically for treatment of GC.[38] Taken together with our present results, h-prune inhibitors, such as dipyridamole, may be effective for the prevention or treatment of h-prune-positive GC without severe adverse effects. The PDE superfamily is large and complex, containing 11 highly related and structurally related gene families and over 60 distinct isoforms. Each of the PDE families contains one to four genes, and many genes generate multiple isoforms.[39] Development of specific h-prune inhibitors is important because dipyridamole also inhibits the activities of PDE5, PDE6, PDE7, PDE8, PDE10 and PDE11.[39]

In conclusion, we found that h-prune is overexpressed in GC and that this overexpression correlates with tumor progression and poor survival in patients with GC. Although the significance of overexpression of nm23-H1 is still unclear, nm23-H1 may contribute to tumor cell motility by upregulating the function of h-prune. Although the precise mechanism by which h-prune regulates cellular motility remains unclear, the efficacy of a combination chemotherapy with 5-fluorouracil, cisplatin and dipyridamole[40] should be investigated in h-prune-positive GC.

Acknowledgments

This work was supported, in part, by Grants-in-Aid for Cancer Research from the Ministry of Education, Culture, Science, Sports, and Technology of Japan, and from the Ministry of Health, Labor, and Welfare of Japan. We thank Masayoshi Takatani and Masayuki Ikeda for excellent technical assistance and advice. This work was carried out with the kind cooperation of the Research Center for Molecular Medicine, Faculty of Medicine, Hiroshima University. We thank the Analysis Center of Life Science, Hiroshima University for the use of their facilities.

References

1 Ohgaki H, Matsukura N. Stomach cancer. In: Stewart BW, Kleihues P, eds. *World Cancer Report*. Lyon: IARC Press, 2003: 194–7.
2 Hohenberger P, Gretschel S. Gastric cancer. *Lancet* 2003; **362**: 305–15.
3 Gupta GP, Massague J. Cancer metastasis: building a framework. *Cell* 2006; **127**: 679–95.
4 Oue N, Hamai Y, Mitani Y *et al.* Gene expression profile of gastric carcinoma: identification of genes and tags potentially involved in invasion, metastasis, and carcinogenesis by serial analysis of gene expression. *Cancer Res* 2004; **64**: 2397–405.
5 Kurayoshi M, Oue N, Yamamoto H *et al.* Expression of Wnt-5a is correlated with aggressiveness of gastric cancer by stimulating cell migration and invasion. *Cancer Res* 2006; **66**: 10 439–48.
6 Oue N, Mitani Y, Motoshita J *et al.* Accumulation of DNA methylation is associated with tumor stage in gastric cancer. *Cancer* 2006; **106**: 1250–9.
7 Shutoh M, Oue N, Aung PP *et al.* DNA methylation of genes linked with retinoid signaling in gastric carcinoma: expression of the retinoid acid receptor beta, cellular retinol-binding protein 1, and tazarotene-induced gene 1 genes is associated with DNA methylation. *Cancer* 2005; **104**: 1609–19.
8 Kobayashi T, Hino S, Oue N *et al.* Glycogen synthase kinase 3 and h-prune regulate cell migration by modulating focal adhesions. *Mol Cell Biol* 2006; **26**: 898–911.
9 D'Angelo A, Garzia L, Andre A *et al.* Prune cAMP phosphodiesterase binds nm23-H1 and promotes cancer metastasis. *Cancer Cell* 2004; **5**: 137–49.
10 Beavo JA, Brunton LL. Cyclic nucleotide research – still expanding after half a century. *Nat Rev Mol Cell Biol* 2002; **3**: 710–18.
11 Reymond A, Volorio S, Merla G *et al.* Evidence for interaction between human PRUNE and nm23-H1 NDPKinase. *Oncogene* 1999; **18**: 7244–52.
12 Steeg PS, Bevilacqua G, Kopper L *et al.* Evidence for a novel gene associated with low tumor metastatic potential. *J Natl Cancer Inst* 1988; **80**: 200–4.
13 Forus A, D'Angelo A, Henriksen J *et al.* Amplification and overexpression of PRUNE in human sarcomas and breast carcinomas – a possible mechanism for altering the nm23-H1 activity. *Oncogene* 2001; **20**: 6881–90.
14 Bevilacqua G, Sobel ME, Liotta LA, Steeg PS. Association of low nm23 RNA levels in human primary infiltrating ductal breast carcinomas with

doi: 10.1111/j.1349-7006.2007.00515.x

lymph node involvement and other histopathological indicators of high metastatic potential. *Cancer Res* 1989; **49**: 5185–90.
15 Florenes VA, Aamdal S, Myklebost O, Maelandsmo GM, Bruland OS, Fodstad O. Levels of nm23 messenger RNA in metastatic malignant melanomas: inverse correlation to disease progression. *Cancer Res* 1992; **52**: 6088–91.
16 Yamaguchi A, Urano T, Goi T *et al.* Expression of human nm23-H1 and nm23-H2 proteins in hepatocellular carcinoma. *Cancer* 1994; **73**: 2280–4.
17 Nakayama H, Yasui W, Yokozaki H, Tahara E. Reduced expression of nm23 is associated with metastasis of human gastric carcinomas. *Jpn J Cancer Res* 1993; **84**: 184–90.
18 Haut M, Steeg PS, Willson JK, Markowitz SD. Induction of nm23 gene expression in human colonic neoplasms and equal expression in colon tumors of high and low metastatic potential. *J Natl Cancer Inst* 1991; **83**: 712–16.
19 Muller W, Schneiders A, Hommel G, Gabbert HE. Expression of nm23 in gastric carcinoma: association with tumor progression and poor prognosis. *Cancer* 1998; **83**: 2481–7.
20 Sobin LH, Wittekind CH, eds. *TNM Classification of Malignant Tumors*, 6th edn. New York: John Wiley & Sons, 2002.
21 Lauren P. The two histological main types of gastric carcinoma: diffuse and so-called intestinal-type carcinoma. An attempt at a histo-clinical classification. *Acta Pathol Microbiol Scand* 1965; **64**: 31–49.
22 Gibson UE, Heid CA, Williams PM. A novel method for real time quantitative RT-PCR. *Genome Res* 1996; **6**: 995–1001.
23 Kondo T, Oue N, Yoshida K *et al.* Expression of POT1 is associated with tumor stage and telomere length in gastric carcinoma. *Cancer Res* 2004; **64**: 523–9.
24 Mantel N. Evaluation of survival data and two new rank order statistics arising in its consideration. *Cancer Chemother Rep* 1966; **50**: 163–70.
25 Friedl P, Wolf K. Tumour-cell invasion and migration: diversity and escape mechanisms. *Nat Rev Cancer* 2003; **3**: 362–74.
26 Kurokawa S, Arimura Y, Yamamoto H *et al.* Tumour matrilysin expression predicts metastatic potential of stage I (pT1) colon and rectal cancers. *Gut* 2005; **54**: 1751–8.
27 Takaoka M, Naomoto Y, Ohkawa T *et al.* Heparanase expression correlates with invasion and poor prognosis in gastric cancers. *Laboratory Invest* 2003; **83**: 613–22.
28 Vauhkonen H, Vauhkonen M, Sajantila A, Sipponen P, Knuutila S. DNA copy number aberrations in intestinal-type gastric cancer revealed by array-based comparative genomic hybridization. *Cancer Genet Cytogenet* 2006; **167**: 150–4.
29 Nomura A, Stemmermann GN, Chyou PH, Kato I, Perez-Perez GI, Blaser MJ. *Helicobacter pylori* infection and gastric carcinoma among Japanese Americans in Hawaii. *N Engl J Med* 1991; **325**: 1132–6.
30 Nomura A, Stemmermann GN, Chyou PH, Perez-Perez GI, Blaser MJ. *Helicobacter pylori* infection and the risk for duodenal and gastric ulceration. *Ann Intern Med* 1994; **120**: 977–81.
31 Bebb JR, Letley DP, Thomas RJ *et al. Helicobacter pylori* upregulates matrilysin (MMP-7) in epithelial cells *in vivo* and *in vitro* in a Cag dependent manner. *Gut* 2003; **52**: 1408–13.
32 Kunisaki C, Shimada H, Nomura M, Matsuda G, Otsuka Y, Akiyama H. Therapeutic strategy for signet ring cell carcinoma of the stomach. *Br J Surg* 2004; **91**: 1319–24.
33 Jones PA, Baylin SB. The fundamental role of epigenetic events in cancer. *Nat Rev Genet* 2002; **3**: 415–28.
34 Toyota M, Ahuja N, Suzuki H *et al.* Aberrant methylation in gastric cancer associated with the CpG island methylator phenotype. *Cancer Res* 1999; **59**: 5438–42.
35 Ushijima T, Okochi-Takada E. Aberrant methylations in cancer cells: Where do they come from? *Cancer Sci* 2005; **96**: 206–11.
36 Hartsough MT, Clare SE, Mair M *et al.* Elevation of breast carcinoma Nm23-H1 metastasis suppressor gene expression and reduced motility by DNA methylation inhibition. *Cancer Res* 2001; **61**: 2320–7.
37 Hejna M, Raderer M, Zielinski CC. Inhibition of metastases by anticoagulants. *J Natl Cancer Inst* 1999; **91**: 22–36.
38 Sakaguchi Y, Maehara Y, Emi Y, Kusumoto T, Kohnoe S, Sugimachi K. Dipyridamole combination chemotherapy can be used safely in treating gastric cancer patients. *Anticancer Drugs* 1991; **2**: 139–43.
39 Cheng J, Grande JP. Cyclic nucleotide phosphodiesterase (PDE) inhibitors: novel therapeutic agents for progressive renal disease. *Exp Biol Med (Maywood)* 2007; **232**: 38–51.
40 Kohnoe S, Maehara Y, Takahashi I, Emi Y, Baba H, Sugimachi K. Treatment of advanced gastric cancer with 5-fluorouracil and cisplatin in combination with dipyridamole. *Int J Oncol* 1998; **13**: 1203–6.

DNA methylation of the *RIZ1* gene is associated with nuclear accumulation of p53 in prostate cancer

Yasuhisa Hasegawa,[1,2] Akio Matsubara,[2] Jun Teishima,[2] Mitsuhiro Seki,[2] Koji Mita,[2] Tsuguru Usui,[2] Naohide Oue[1] and Wataru Yasui[1,3]

Departments of [1]Molecular Pathology and [2]Urology, Hiroshima University Graduate School of Biomedical Sciences, Minami-ku, Hiroshima 734-8551, Japan

(Received June 2, 2006/Revised August 31, 2006/Accepted September 3, 2006/Online publication October 19, 2006)

The retinoblastoma protein-interacting zinc finger gene, *RIZ1*, is thought to be a tumor suppressor gene. *RIZ1* is inactivated by mutation, deletion and DNA methylation in several human cancers. In the present study, the relationship between DNA methylation of *RIZ1* and mutation of *p53* was investigated in prostate cancer (PCa). In total, 47 cases of node-negative PCa (stages I–III) were analyzed. DNA methylation of the *RIZ1* gene was detected in 20 (42.6%) of the 47 PCa tissues by methylation-specific polymerase chain reaction. DNA methylation of the *RIZ1* gene was not associated with clinicopathological features. DNA methylation of *RIZ1* tended to be present more frequently in PCa specimens with a high Gleason score (16/30, 53.3%) than in those with a low Gleason score (4/17, 23.5%); however, this tendency was not statistically significant ($P = 0.0675$). Nuclear accumulation of p53 was observed in four (8.5%) of 47 PCa specimens by immunostaining. All four PCa specimens with nuclear accumulation of p53 were stage III disease and showed DNA methylation of *RIZ1*. However, of the remaining 43 cancers without nuclear accumulation of p53, DNA methylation of *RIZ1* was observed in only 16 (37.2%) specimens ($P = 0.0272$). Of the three PCa cell lines, only the PC3 cell line showed loss of *RIZ1* mRNA due to DNA methylation, and this loss was rectified by treatment with a demethylating agent, 5-Aza-2′-deoxycytidine. These results suggest that transcriptional inactivation of *RIZ1* by aberrant DNA methylation may contribute to prostate carcinogenesis. Genetic alterations are likely associated with epigenetic alterations in PCa. (*Cancer Sci* 2007; 98: 32–36)

Prostate cancer (PCa) is one of the most common cancers and the second leading cause of cancer death in men in the USA.[1] An understanding of the genetic and epigenetic pathways involved in the pathogenesis of PCa is essential for development of improved diagnostic and treatment modalities. A variety of genetic and epigenetic alterations are associated with PCa.[2,3] Epigenetic changes, such as DNA methylation of CpG islands, are detected commonly in human cancers. Hypermethylation of CpG islands is associated with silencing of many genes, especially defective tumor-related genes, and has been proposed as an alternative way to inactivate tumor-related genes in human cancers.[4,5] Identification of methylated genes may be useful in the diagnosis and treatment of PCa and may provide insight into prostate carcinogenesis. Prior studies have shown that DNA hypermethylation is a crucial mechanism in transcriptional silencing of tumor-related genes in PCa.[6,7]

The retinoblastoma protein-interacting zinc finger gene, *RIZ1*, was isolated with a functional screen for retinoblastoma (Rb)-binding proteins.[8] Domain analysis suggested that RIZ1 is a histone methyltransferase (HMT) specific for the lysine 9 residue of histone H3, an activity known to be linked with transcriptional repression.[9] *RIZ1* is considered to be a tumor suppressor gene because it can induce G_2–M arrest and apoptosis of several types of cancer cells.[10,11] *RIZ1* plays an important role in human cancers, as evidenced by genetic mutations.[12–14] The *RIZ1* gene is located on human chromosome 1p36, a region deleted in many human cancers,[15] and chromosome 1p36 is a potential hereditary PCa susceptibility locus.[16] In addition to genetic alterations, DNA methylation of *RIZ1* has been shown to be a common mechanism for inactivation of *RIZ1* expression in human cancers.[17,18] In PCa, DNA methylation of *RIZ1* is present in 31% of tumor tissues.[19]

A knockout study showed that *RIZ1* is a tumor susceptibility gene in mice.[14] *RIZ1* and *p53* deficiencies likely cooperate in tumor formation in mice and are expected to occur in human cancers as well.[14] In fact, many sporadic human cancers carry both *p53* mutations and a silenced *RIZ1* gene.[10,14] The *p53* gene is involved in the tumorigenesis of many human cancers,[20] including PCa.[21] p53 functions as a transcriptional regulator involved in G_1 phase growth arrest of cells in response to DNA damage. p53 also has roles in regulation of the spindle checkpoint, centrosome homeostasis and G_2–M phase transition.[22] Several lines of evidence suggest associations between genetic and epigenetic alterations. *p53* mutations have been found frequently in colorectal and gastric cancers without DNA methylation.[23,24] However, the association between genetic and epigenetic alterations has not been investigated in PCa.

In the present study, we investigated the relationship between *RIZ1* methylation status and *p53* mutation status in 47 PCa tissues. To determine whether transcriptional silencing of the *RIZ1* gene is caused by DNA hypermethylation, we compared the methylation status with expression of *RIZ1* mRNA in PCa cell lines.

Materials and Methods

Tissue samples. Subjects were 47 patients with PCa who were referred to the Department of Urology, Hiroshima University Hospital (Hiroshima, Japan). Forty-seven PCa tissues from these 47 patients were analyzed for DNA methylation of *RIZ1* and localization of p53. PCa samples were obtained by radical prostatectomy, and all PCa cases were confirmed to be node negative by pathological examination. None of the 47 patients with PCa received preoperative treatment. All 47 specimens were archival, formalin-fixed, paraffin-embedded tissues. It was confirmed microscopically that the tumor specimens consisted mainly (>50%) of cancer cells. Tumor staging was according to the TNM classification system.[25] In the present study, PCa were graded by the reporting pathologists on the radical surgery specimen, according to the system of the Gleason score.[26] After prostatectomy, the serum prostate-specific antigen (PSA) level was measured by *E*-test Tosoh II Assay (Tosoh, Tokyo, Japan). Patients were followed up by PSA measurement monthly during the first 6 months after prostatectomy and then every 3 months

[3]To whom correspondence should be addressed. E-mail: wyasui@hiroshima-u.ac.jp

doi: 10.1111/j.1349-7006.2006.00338.x

thereafter. Biochemical relapse was defined as a PSA level of 0.2 ng/mL or greater. Because written informed consent was not obtained, for strict privacy protection, identifying information for all samples was removed before analysis. This procedure was in accordance with the Ethical Guidelines for Human Genome/Gene Research of the Japanese Government.

Cell lines and drug treatment. LNCaP, PC3 and DU145 PCa cell lines were purchased from American Type Culture Collection (Manassas, VA, USA). All cell lines were maintained in RPMI-1640 (Nissui Pharmaceutical, Tokyo, Japan) containing 10% fetal bovine serum (Whittaker, Walkersville, MD, USA) in a humidified atmosphere of 5% CO_2 and 95% air at 37°C. Cells were treated with a final concentration of 1 μM 5-aza-2′-deoxycytidine (Aza-dC; Sigma Chemical, St Louis, MO, USA) for 5 days before they were harvested for DNA or RNA extraction.

Genomic DNA extraction and methylation-specific polymerase chain reaction. For extraction of DNA from the archival, formalin-fixed, paraffin-embedded tissue samples, PCa samples were dissected manually from different sets of 10 serial, 10 μm-thick, formalin-fixed, paraffin-embedded tissue sections with a fine needle. The dissected samples were lysed by incubation in 200 mg/mL proteinase K at 55°C for 3 days. Genomic DNA was purified by three rounds of phenol–chloroform extraction followed by ethanol precipitation. For DNA extraction from cell lines, genomic DNA was extracted with a Genomic DNA Purification Kit (Promega, Madison, WI, USA). To examine the DNA methylation pattern, genomic DNA was treated with 3 M sodium bisulfite, as described previously.[27] For analysis of DNA methylation of the *RIZ1* gene, methylation-specific polymerase chain reaction (MSP) was carried out as described previously.[17] Polymerase chain reaction (PCR) products (15 μL) were loaded onto 8% non-denaturing polyacrylamide gels, stained with ethidium bromide, and visualized under ultraviolet light.

Immunohistochemistry. Formalin-fixed, paraffin-embedded samples were sectioned, deparaffinized, and stained with hematoxylin–eosin to ensure that the sectioned block contained tumor cells. Adjacent sections were then stained immunohistochemically. For immunostaining of p53, a Dako LSAB Kit (Dako, Carpinteria, CA, USA) was used in accordance with the manufacturer's recommendations. In brief, sections were pretreated by microwaving in citrate buffer for 30 min to retrieve antigenicity. After peroxidase activity was blocked with 3% H_2O_2–methanol for 10 min, sections were incubated with normal goat serum (Dako) for 20 min to block non-specific antibody binding sites. Anti-p53 antibody (DO7, 1 : 100; Novocastra, Newcastle, UK) was incubated with tissue samples for 60 min at room temperature followed by incubations with biotinylated antimouse IgG and peroxidase-labeled streptavidin for 10 min each. Staining was completed with a 10-min incubation with the substrate–chromogen solution. The sections were counterstained with 0.1% hematoxylin. p53 staining was classified according to the percentage of stained cancer cells. When more than 10% of cancer cells were stained, the immunostaining was considered positive.

PCR-single-strand conformation polymorphism analysis. Exons 5–8 of the *p53* gene were examined for mutations by PCR–single-strand conformation polymorphism (SSCP) analysis with 10 sets of primers, as described previously.[28] Each target sequence was amplified in a 20-μL reaction volume containing 10–20 ng genomic DNA, 0.2 μM dNTP, 10 mM Tris-HCl (pH 8.3), 50 mM KCl, 2 mM $MgCl_2$, 0.3 μM of each primer and 0.2 μL of Ampli Taq Gold (Applied Biosystems, Foster City, CA, USA). PCR amplification consisted of 35 cycles of 94°C for 30 s, 60°C or 55°C for 30 s, and 72°C for 30 s after the initial activation step of 94°C for 10 min. PCR products were diluted 10-fold with formamide dye solution, denatured at 85°C for 10 min, and separated by electrophoresis on 6% polyacrylamide gels. Gels were stained, and bands were visualized with a Silver Staining II kit (WAKO, Osaka, Japan).

Reverse transcription–polymerase chain reaction. Expression of *RIZ1* mRNA was analyzed by reverse transcription (RT)-PCR. Total RNA was extracted with an RNeasy Mini Kit (Qiagen, Valencia, CA, USA), and 1 μg of total RNA was converted to cDNA with a First-Strand cDNA Synthesis Kit (Amersham Biosciences, Piscataway, NJ, USA). Primer sequences and amplification conditions were as described previously.[18] RT-PCR products were subjected to 1.5% agarose gel electrophoresis, stained with ethidium bromide, and examined under ultraviolet light. *ACTB*-specific PCR products were amplified from the same RNA samples and served as internal controls.

Statistical methods. Associations between clinicopathological parameters and DNA methylation of *RIZ1* were analyzed by Fisher's exact test. A *P*-value of less than 0.05 was considered statistically significant.

Results

DNA methylation of *RIZ1* and p53 mutation status in PCa tissues. DNA methylation status of the *RIZ1* gene was examined in a total of 47 PCa tissue specimens from 47 patients. DNA methylation of *RIZ1* was detected in 20 (42.6%) of 47 PCa tissues. Representative results of MSP for *RIZ1* are shown in Fig. 1A. No association was detected between the methylation status of

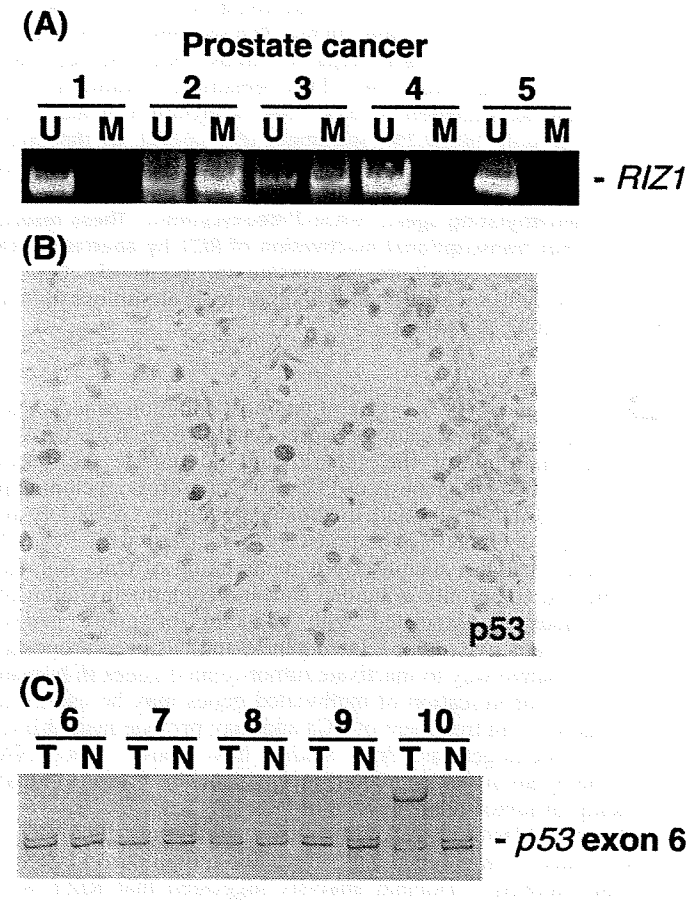

Fig. 1. (A) Methylation-specific polymerase chain reaction (PCR) of *RIZ1* in prostate cancer (PCa). Methylated *RIZ1* was detected in two cases (cases 2 and 3) of PCa. U, unmethylated PCR product; M, methylated PCR product. (B) Immunostaining of p53 in PCa. Nuclear accumulation of p53 was observed in PCa cells. Original magnification, ×400. (C) PCR–single-strand conformation polymorphism analysis of *p53*. A *p53* mutation was detected in one case (case 10).